COLOR CONTRAST DETECTION IN SPATIAL CHROMATIC NOISE

DIPLOMA PROJECT

GIANLUCA MONACI

Supervision:
GLORIA MENEGAZ
SABINE SUSSTRUNK
Collaboration:
KENNETH KNOBLAUCH, INSERM, Lyon, France

Lausanne, EPFL
August 2002

Table of Contents

List of Figures

List of Tables

Abstract

In this report, *higher order color mechanisms* for the *detection* of *spatial* distributions of color are investigated. The objective of this work is to understand which are the visual mechanisms involved in chromatic detection tasks and to define the properties of such mechanisms.

Despite great investigation efforts, human color vision is far from being satisfactorily explained. It is still not clear which mechanisms, at a post-receptoral level, mediate color detection. Recently, psychophysical studies have argued that the cone-opponent signals are further processed by *higher order chromatic mechanisms*, sort of multiple channels tuned to a variety of directions in the color space [3–8]. A better understanding of chromatic detection mechanisms could enable the development of perceptual image quality metrics and the evaluation of chromatic noise masking effects.

The mechanisms responsible for the detection of monochromatic signals have been described developing a psychophysical experiment. Such mechanisms have been characterized estimating contrast thresholds for the detection of a chromatic signal within a color spatial distribution using a *sectored noise masking technique*. The experiment was designed in the DKL color space, thus both signal and noise mask were defined in that space. Sectored noise draws samples from a sector of variable width in an equiluminant plane of the DKL color space. Such a sector is oriented along the same chromatic axis of the signal. Sector amplitude and width and test color direction were under experimental control. Observers were asked to detect a signal, a monochromatic Gaussian pulse, within a sectored noise. Contrast thresholds for the detection of red, light reddish, orange and yellow signals were measured. Estimating the potency of noise masking as a function of noise sector width, it is possible to distinguish directly between detection mechanisms that combine the photoreceptoral inputs in a linear or nonlinear fashion. In fact, a mechanism tuned to a certain color direction that combines the cone signals linearly is not influenced by the noise components orthogonal to such a direction, that is, by the width of the noise sector. On the other hand, nonlinear mechanisms should be affected by the variation of sector width.

In this report we carefully detail all the steps followed to develop our psychophysical experience. In our experiment, thresholds were found not to depend on noise sector width, consistently with the hypothesis of linear mechanisms operating for the detection of specific colors.

Chapter 1

Introduction

1.1 Problem Statement

In this work, we focus our attention on *higher order color mechanisms* for the *detection* of *spatial* patterns.

The perception of spatial chromatic distributions - simple two-color patterns, textures or complex images - has been intensively studied for a long time. There is general agreement on the fact that color information is processed by hierarchical mechanisms: the inputs from three types of cone photoreceptors, each with its own photopigment, at the first stage are combined to form three opponent signals at the second level. This simple scheme, however, is not sufficient to explain the great number of visual phenomena that have been observed during researches on human vision. The mechanisms involved in color perception and detection are complex and they are still far to be satisfactorily explained. These hypothesized mechanisms operating at *higher* level in the color information processing hierarchy are known as *higher order color mechanisms*.

Results of psychophysical chromatic detection experiments have typically been interpreted in terms of red-green (R-G) and yellow-blue (Y-B) detection mechanism combined with a non-opponent luminance mechanism. Recently, the classical notion of chromatic information encoded by the visual system along opponent channels, has been debated by reports of psychophysical studies showing the evidence for *chromatic mechanisms tuned to specific directions in the color space* [3–8]. These studies basically focus on two main questions:

- *Are there chromatic detection mechanisms sensible to directions in the color space that lie between those of the three standard mechanisms?*
- *Do the detection mechanisms combine the cone photoreceptoral inputs in a linear or nonlinear fashion?*

In the presented work, we face these topics transposing in the spatial domain the paradigm that D'Zmura and Knoblauch used to investigate chromatic detection mechanisms in the temporal domain [3].

1.2 Investigated Approach

In this project, we have set up a psychophysical experiment, in order to investigate the behavior of human visual system in color detection tasks.

In order to set up a psychophysical experiment, an extensive analysis of psychophysical studies on color contrast detection in the literature has been carried out. The analysis has led to the investigation of an approach based on the use of contrast threshold measurements to describe the properties of color detection mechanisms. A relevant part of our work consists in a preliminary study of the fundamental concepts in the field of color, color spaces and vision phenomena. This step is required, in order to exhaustively understand the basis of human visual system processing and in order to properly develop a psychophysical test.

The goal of our investigation is to better understand the mechanisms that control the detection of chromatic spatial distributions. Threshold measurements are performed using a *sectored noise masking technique*, to characterize the properties of human color detection mechanisms. The experiment was designed in the DKL color space, thus both signal and noise mask were defined in that space. Sectored noise chromaticities were randomly sampled from a sector of variable width in the equiluminant plane of the DKL color space. The sector lies along the direction defined by the chromaticity of the test signal. Detection thresholds for monochromatic signals red, light reddish, orange and yellow were estimated using a *staircase* procedure with a *two alternative forced choice* method.

Measuring the efficacy of noise masking as a function of sector width, it is possible to distinguish between linear detection mechanisms, that is that combine cone signals linearly, and nonlinear detection mechanisms. In fact, since a linear mechanism tuned to a certain direction of the color space can be represented as a vector in the DKL space, the response of such a mechanism to a given stimulus is given by the dot product between those two vectors representing the mechanism and the stimulation. Thus, the noise components orthogonal to the mechanism direction do not affect the mechanism behavior itself. This means that increasing the noise sector width, since the noise component that varies is the one orthogonal to the test signal direction, the performances of a linear detection mechanism should not vary. On the other hand, a variation of noise sector width is expected to influence the behavior of a non linear detection mechanism.

The results from our experiments have confirmed the model proposed by D'Zmura and Knoblauch: color detection seems to be mediated by higher order color mechanisms that combine the cone signals in a linear fashion. Such mechanisms are sensible not only to the colors indicated by the cardinal directions, but also to *intermediate* colors that are indicated by axes that lie between those that are cardinal.

An important part of this work is therefore the analysis and evaluation of the data obtained with the psychophysical tests. An overview of different models of higher order color mechanisms is provided, together with the tools that have been developed for the analysis of the results.

The method presented in this report details the steps to follow for the development of this psychophysical experience. We intend, with its description, to show an accurate

procedure that can be developed in a wider context. The work we present demonstrates the major themes and ideas on which the proposed approach is based.

1.3 Organization of the Report

This report is organized as follows. In **Chapter 2**, the principal aspects concerning human visual system are discussed. The main features of the human visual pathway, from the retina to the visual cortex, are exposed. In the second part of the chapter, we introduce the basis of colorimetry and we describe various color spaces, with particular attention to the DKL color space, which is the color space we have used to describe our experiment. Vision phenomena are described from a macroscopical point of view in **Chapter 3**. Low-level and high-level vision phenomena are analyzed and the subject of our work, the *higher order color mechanisms*, is introduced. **Chapter 4** introduces the ideas used to design the psychophysical experiment. The characteristics of the *linear mechanisms* are analyzed and the *sectored noise masking technique* is detailed. Moreover, in this chapter we describe the protocol of the experiment. In **Chapter 5**, the tools developed for the analysis and the interpretation of the experimental data are introduced. The results are presented, evaluated and discussed. **Chapter 6** contains the conclusions, the presentation of possible improvements of the analyzed method and an outlook on future developments of the work presented in this report.

Chapter 2

Foundations of Color Vision

2.1 Introduction

Color is in the mind, not in the physical world. Color vision creates a unique dimension to sight that is impossible to appreciate by any non-visual means. It is an illusion of reality resulting from a comparison of the responses of nerve cells in our brain. In this chapter, the most important physiological structures involved in the vision task are reviewed. The tools that we use to describe and measure color stimuli are also reviewed.

In section 2.2 the human eye, its anatomy and its characteristics are described. Still in that section, we show the main features of the human visual pathway. Section 2.3 draws the basis of colorimetry, the science of color measuring and specifying. Here the most important color spaces are presented.

2.2 *What is color?*

Color and all vision are in a sense *illusory*, depending only on signals that pass between millions of neurons that reside within our skull. Color is our perceptual response to a very narrow span (less than 1%) of the total electromagnetic radiation emitted by the sun. In fact, we perceive as *visible light* just electromagnetic energy having wavelengths in the range 380-750 nm. The quantum particles of light are called *photons*. The invisible radiation at higher energies (at wavelengths shorter than 380 nanometers) is called *ultraviolet* and includes x-rays and gamma rays. Lower energy radiation (at wavelengths longer than 750 nanometers) is called *infrared* or heat; beyond heat are microwaves, television and radio waves.

2.2.1 Human Visual System

Vision is possible, and largely influenced by, thanking the eye (see fig. 2.1). At the largest scale, the eye is essentially an optical camera, equipped with a lens to focus light onto a photosensitive surface in its interior, in the same way a camera focuses light onto film.

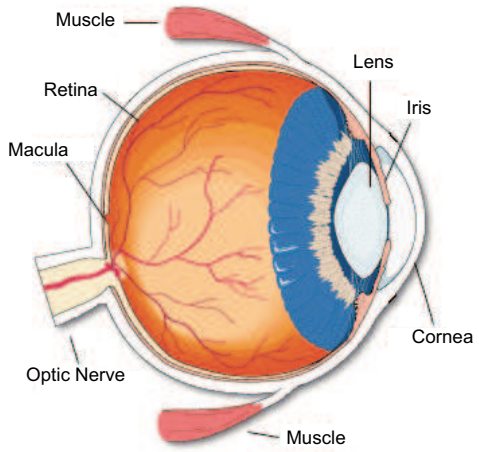

Figure 2.1: Schematic diagram of the human eye.

The *lens* and its transparent covering, the *cornea*, act as a compound lens to focus the image. The cornea is the most important component of the eye in forming the image as it is the curved interface with outer world. Between the cornea and the lens, the *aqueous humor*, which is essentially water, provides a gentle pressure to maintain the optical shape of the retina.

The lens is a flexible transparent structure that varies in index of refraction. It as a natural round shape but is pulled taut by the tension of *zonule fibers*. The image can be adjusted to focus on near or distant objects by the *ciliary muscles* attached to the circumference of the lens. These muscles contract to let the front of the lens assume a more rounded shape, shortening the focal length when gazing at a nearby object, or relax, letting the lens become "flatter" when looking at far away objects.

The *pupil* is the aperture in the eye and its size is controlled by a light sensitive *iris*, a sphincter muscle. The iris is pigmented, giving the eye his characteristic color; it opens or closes like an aperture to reduce variation in the amount of light entering the eye. However, pupil size can vary depending also on nonvisual phenomena; thus it is difficult to predict it exactly. In practical situations, pupil diameter varies approximately from 3 mm to 7 mm.

Between lens and retina a viscous liquid called *vitreous humor* maintains the pressure higher than that of the atmosphere to preserve the rounded shape.

At the back of the eye, the *retina*, a thin layer of nerve tissue, collects and processes visual information before sending it on to the brain. The retina also contains the tiny blood vessels that nourish the retinal tissue.

Vision really begins here, in the *photoreceptor cells*: they transduce the information present in the optical image into chemical and electrical signals. More detailed characteristics of the retina and photoreceptors will be discussed later.

The last important part of the eye is the *optic nerve*. It is made up of *axons*, the output of the *ganglion cells*, the last level of neural processing in the retina. It is important to emphasize that while the number of photoreceptors is approximately 130 millions, the

optical nerve is composed of about one million fibers carrying information. According to most hypotheses, there is a great compression of data at this level before sending the visual signal to the higher hierarchical levels of the visual system. Where the optic nerve is formed there is no room for photoreceptors, thus no visual stimulation can occur. This little region of the retina is called *blind spot*.

The Retina

Fig. 2.2 shows the principal components of the human retina.

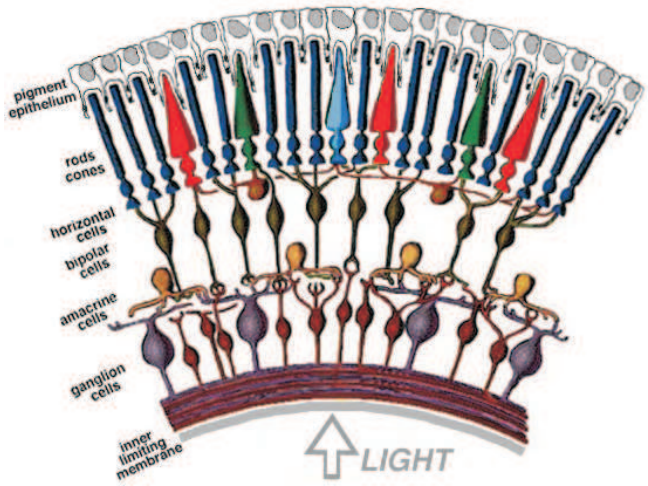

Figure 2.2: Schematic diagram of the retina.

The retina is organized into three primary layers:

1. The *photoreceptive layer*, made up of *rods* and *cones*. The rods and cones synapse with the bipolar cells in the second layer of the retina.

2. The *bipolar cell layer*: bipolar cells send appendages to communicate with both the first and third layer. *Amacrine* and *horizontal cells* located in this second layer contribute to the finer processing of visual information via lateral connections. These lateral connections modulate the transmission of information across the synaptic layers of the retina, between the first and second layer and between the second and third layer.

3. The *ganglion cell layer*. The axons of the ganglion cells found in the third layer of the retina convey the visual information as encoded by the retina to the next synapse point in the visual pathway via the optic nerve.

This complex network of neurons takes the transduced visual information and processes it via encoding, compression, integration, and convergence.

The *visual center* of the eye is at the exact focal point behind the lens. The most important area on the retina, is the *fovea*, which specializes in the perception of contrasty edges at an extremely high level of detail. To achieve this, the foveal cones are very densely packed - over 160,000 cones per square millimeter. This tight packing is possible because the photoreceptor cells are very thin and long. Visual clarity is also enhanced by thinning the retina over the fovea, which creates a small depression that shields the foveal cones from extraneous light scattered inside the eye. Most important, the retina contains specialized cells and network connections that amplify the contrast in light and dark between neighboring cells in the retina, increasing edge definition. When we look at an object in our visual field, we move our head and eyes so that the object falls on the fovea. Outside the fovea, the cones become "fatter" and less densely packed, reducing the apparent brightness and resolution of the image where the curved surface of the eye makes it impossible for the lens to provide a crisp image.

Four Types of Photoreceptors

Vision is possible because four types of photoreceptors positioned in the retina transduce arriving photons - or quanta - into appropriate electrical signals.

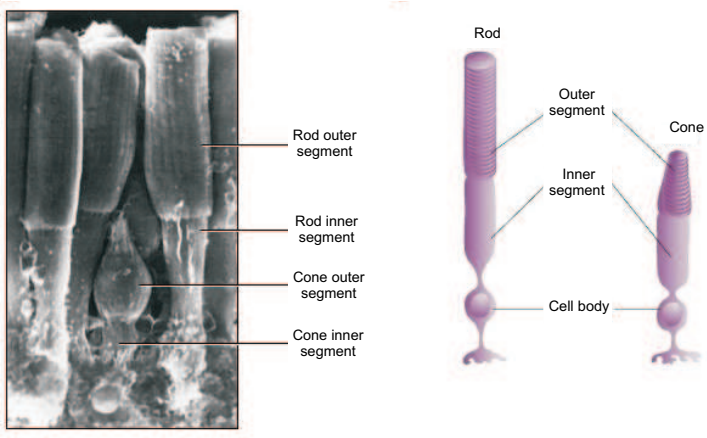

Figure 2.3: Rod and cone photoreceptors.

The *rods* (see fig. 2.3), long and slander, provide *scotopic vision* as they are more effective at low light levels. Rods detect very small amounts of lights: a single photon can produce a signal. Because of the presence of a single photopigment, the *rhodopsin*, in scotopic conditions objects can only be seen as shades of gray.

The three types of *cones* on the other hand are more effective at high light levels and provide *photopic vision*. Humans have three different chemicals that bind to cone cells and make those cells sensitive to light of a particular wavelength or color. These photo-chemicals are coded for by three genes on the X chromosome. Defects in one or more of these opsin genes can cause color blindness, usually in males. This happens

because the genes for photopigments are present in the X chromosome. Females inherit one X chromosome from the mother and one from the father, while males inherit just one X chromosome from their mother. In order to produce normal color vision, only one chromosome with the genes for the normal photopigments is needed. Thus, females have a double of the normal genes that can ensure a correct trichromatic vision. If a female is color deficient, it means that she has two deficient X chromosomes and all male children are destined to have color-vision deficiency.

The three cones are the foundations of our color vision as they respond differently to lights of different wavelengths. The cones are referred to as L, M or S to represent the fact that their relative spectral sensitivity peak at long, middle and short wavelengths, respectively. The specific sensitivities of each type of photoreceptor are shown in fig. 2.4 as estimated by Stockman and Sharpe [9].

The cone spectral sensitivities $\overline{l}_\lambda, \overline{m}_\lambda, \overline{s}_\lambda$, are defined as linear combinations of the Stiles and Burch [10] 10-degrees color matching functions, $\overline{r}_\lambda, \overline{g}_\lambda, \overline{b}_\lambda$. Their derivation requires the knowledge of the five unknowns, $\overline{s}_G/\overline{s}_B, \overline{m}_R/\overline{m}_B, \overline{m}_G/\overline{m}_B, \overline{l}_R/\overline{l}_B$ and $\overline{l}_G/\overline{l}_B$, in the following equations:

$$\begin{bmatrix} k_l\overline{l}_\lambda \\ k_m\overline{m}_\lambda \\ k_s\overline{s}_\lambda \end{bmatrix} = \begin{bmatrix} \frac{\overline{l}_R}{\overline{l}_B} & \frac{\overline{l}_G}{\overline{l}_B} & 1 \\ \frac{\overline{m}_R}{\overline{m}_B} & \frac{\overline{m}_G}{\overline{m}_B} & 1 \\ 0 & \frac{\overline{s}_G}{\overline{s}_B} & 1 \end{bmatrix} \begin{bmatrix} \overline{r}_\lambda \\ \overline{g}_\lambda \\ \overline{b}_\lambda \end{bmatrix} \tag{2.1}$$

Stockman, Sharpe and Fach [11] and Stockman and Sharpe [9] estimated the five unknowns from L- and M-cone spectral sensitivity measurements in single-gene red-green dichromats, S-cone spectral sensitivity measurements in blue cone monochromats and normals, and from existing color matching data. The estimates are $\overline{s}_G/\overline{s}_B = 0.010600$ for S; $\overline{m}_R/\overline{m}_B = 0.168926$ and $\overline{m}_G/\overline{m}_B = 8.265895$ for M and $\overline{l}_R/\overline{l}_B = 2.846201$ and $\overline{l}_G/\overline{l}_B = 11.092490$ for L. The values of k_l, k_m and k_s, the absolute values of which are unknown, are such that the amplitude of the three curves are normalized to one.

Stockman et al. [11] were unable to measure S-cone spectral sensitivity data after 615 nm, after which $\overline{s}_\lambda$ is so small that it can be reasonably, for most purposes, set to zero.

The cones, as any other detector of radiation, integrate the light to which they are sensible, thus the entire spectrum of incident light is reduced to three signals, one for each cone, resulting in what is called *trichromacy*.

Photons are absorbed by the cones with a probability depending on their wavelength, and, once they are absorbed, their effect is independent of wavelength. Individual photoreceptors are then color blind since their output change only according to the number of quanta absorbed. This important property of the cones is called *univariance*.

Of great interest is the distribution of the three types of cones in the retina (see fig. 2.5): M cones are estimated to be 20 times more numerous than S cones, and L cones twice as numerous than M cones, which is, 40 times as many S cones [12]. Moreover, S cones are completely absent in the central area of the fovea. The rods are not present in the fovea, while they are largely distributed all over the retina: in fact the number of rods is much greater than that of the cones (about 120 millions versus 7 millions) [12].

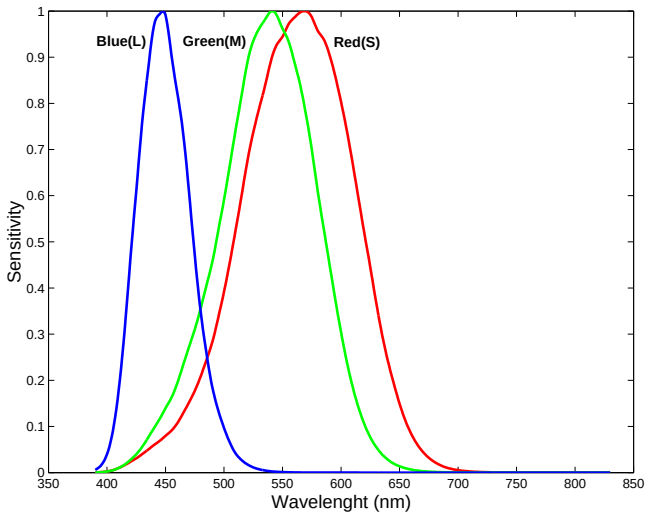

Figure 2.4: Normalized sensitivity curves for the three cones.

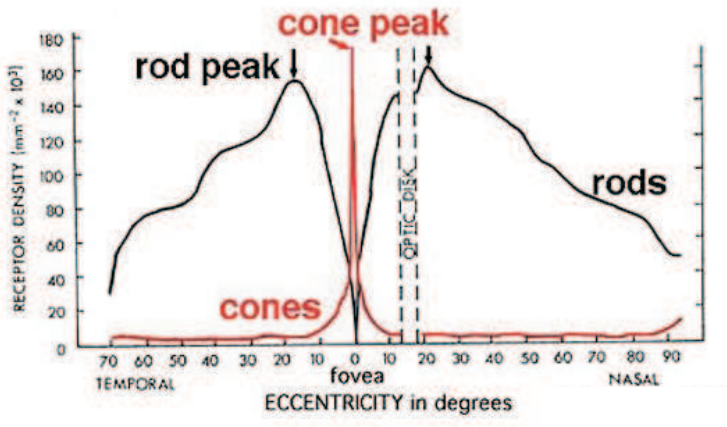

Figure 2.5: Distribution of rod and cone photoreceptors on the retina.

This might seem strange since cones provide high visual acuity at high luminance levels while rods produce reduced visual acuity. However, two aspects have to be considered: first, the rods are sparsely distributed in a larger area to catch every photon in conditions of scotopic vision, while the cones are concentrated in the fovea to produce the highest possible spatial acuity; second, a single cone feeds into ganglion cell signal, while hundreds of rods feed into a ganglion cell, in order to increase sensitivity instead of acuity.

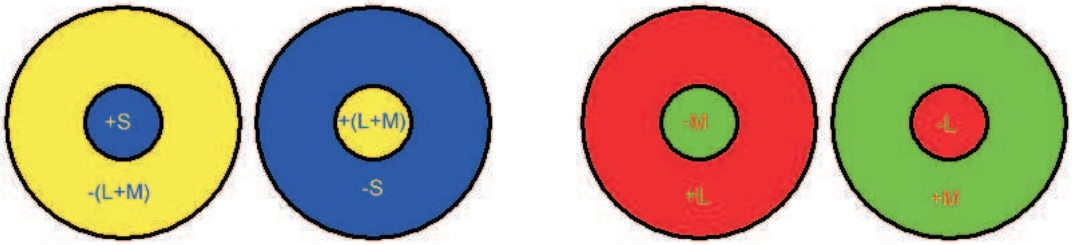

(a) (b)

Figure 2.6: Example of typical center-surround antagonistic receptive fields: (a) on-center yellow-blue receptive fields; (b) off-center red-green receptive fields.

Receptive Fields

There are many millions of receptors in the retina. There is only about one million optic nerve fibers sending visual signals up to the high brain centers. Consequently, individual receptors do not have private lines up to the visual cortex. Rather, multiple receptors converge on to subsequent neural units on their way to the higher visual centers. This convergence results in a physiological concept known as *receptive fields*. The receptive field of a neuron is a map which shows the area of the receptors that respond in an excitatory fashion and those areas that respond in an inhibitory fashion. To put it another way, a receptive field is the receptor area which, when stimulated, results in a response of a particular sensory neuron.

Fig. 2.6 shows some prototypical receptive fields. Neural cells with responses like those represented in fig. 2.6(a) are called *on-center cells*, while those whose response is shown in fig. 2.6(b) are called *off-center cells*.

The concept of receptive field is not only limited to ganglion cells in the retina, but is also applies to neurons in the later stages of the visual system.

When forming receptive fields, individual cone signals can either add together or be subtracted one from the other. Because of the fact that the L, M and S cones have different spectral sensitivities, different numbers and different spatial distributions across the retina, receptive fields have quite different properties. As a convenient simplification, the existence of three types of color receptive fields is assumed, called *opponent channels* (see fig. 2.7). The black-white or achromatic channel results from the sum of the signals coming from L and M cones (L + M). It has the highest spatial resolution. The red-green channel is mainly the result of the M cones signals being subtracted from those of the L cones (L - M). Its spatial resolution is slightly lower than that of the achromatic channel (L + M - S). Finally the yellow-blue channel results from the addition of L and M and subtraction of S cone signals. It has the lowest spatial resolution.

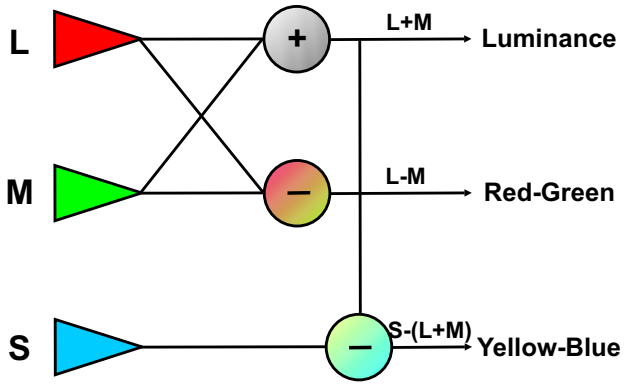

Figure 2.7: Schema of cones interconnections in the retina, leading to opponent-type signals.

2.2.2 Visual Pathway

After an optical image is transduced in chemical and electrical signals at the photoreceptors level, retinal neurons such as horizontal, amacrine, bipolar and ganglion cells process these signals. At this step the axons of the ganglions gather to form the optic nerve that brings the visual information to the *lateral geniculate nucleus* (LGN) in the thalamus (see fig. 2.8). This nucleus serves as a relay station between the eyes and the *primary visual cortex*.

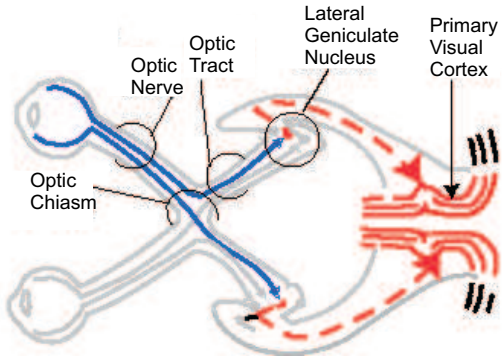

Figure 2.8: Schematic diagram of the visual pathway from the retina to the primary visual cortex.

The LGN cells, after collecting input from the ganglions, project to the primary visual cortex (V1) in the occipital lobe of the cortex. At this point, the signal processing becomes more and more complicated. Following processing in this region, the visual neuronal impulses are directed to the secondary visual cortex or V2. V2 then projects to V3, V4, and V5. Each of these areas is further subdivided and sends information to any of the

20 or more other areas of the brain that process visual information. Somewhere in this complex network, our ultimate perceptions are formed.

2.3 Colorimetry

2.3.1 Introduction

In the nineteenth century the *trichromatic theory of color vision* has been developed by Helmholtz [13] and Young [14], based upon the *color-matching experiments* of Maxwell [15]. They stated that there must be three different types of photoreceptors sensible to red, green and blue light, respectively. According to that theory, the light arriving into the eye is decomposed into three signals by the receptors and sent to the brain where it is further processed. If there is no doubt that three different types of photoreceptors which are sensible approximately to red, green and blue light are disposed in the human retina, the simple explication of three channels bringing each one a monochromatic image to the brain is inefficient and inadequate to explain some attitudes of the HVS.

In 1878, the Austrian physiologist Ewald Hering proposed the *opponent-colors theory* [16], in apparent contradiction with Young-Helmholtz trichromatic theory. Hering advanced his theory to explain various phenomena that could not be adequately accounted for by trichromacy. Examples of such phenomena are the *after-image* effect (if the eye is adapted to a yellow stimulus the removal of the stimulus leaves a blue sensation or after-effect), the fact that some hues were never perceived to appear together (such as red-green or blue-yellow) and also the non-intuitive fact that an additive mixture of red and green light gives yellow and not a reddish-green. Hering proposed that yellow-blue and red-green represent *opponent signals*. This went someway towards explaining why there were *four* psychophysical color primaries (red, green, yellow, and blue) and not only three, or why people with color vision deficiencies loose the ability to distinguish hues in yellow-blue or red-green pairs. To explain such observations, he proposed a model consisting of three different receptors with a bipolar response to yellow-blue, red-green, light-dark pairs. At his time, Hering's theory was considered implausible and did not receive appropriate acceptance.

In the twentieth century, Hering's theory was revaluated because quantitative data supporting it appeared. Jameson and Hurvich [17] were able to put Hering's phenomenologically based theory onto a quantitative basis. They reasoned that they could make use of the antagonistic relationships between yellow-blue and red-green to measure, through their chromatic cancellation experiment, the relative spectral sensitivities of opponent pathways. DeValois et al. in 1958 [18] found opponent physiological signals in the LGN cells of the macaque monkey. The Young-Helmholtz - Hering dispute has an interesting resolution: both are plausible on a physiological basis. There are only three receptors types in most human eyes. Color vision is trichromatic at the photoreceptor level. The opponent processes foreseen by Hering enter at the level of the ganglion cells of the retina, and are a feature of LGN and cortical processing of color. Neurons of the retina encode

the color into three opponent signals. The output of the three cone types are combined to form the achromatic signal (L + M), the red-green signal (L - M) and the yellow-blue signal (- L - M + S).

In this section, we describe how color is specified and measured, according to a *trichromatic* approach, referred to the first level of human visual processing, or to an *opponent processing* approach.

2.3.2 Systems Based on Color Matching

The simplest way of specifying colors is to use a *color-matching experiment* (see fig. 2.9 (a)). The color to be reproduced must match the color of a sample viewed and illuminated under a specific set of conditions. The observer views a *bipartite field* (see fig. 2.9 (b)) with a test light $\mathbf{t}$ of a given *monochromatic* spectral power distribution on one side. On the other half of the visual field, a mixture of three primary lights, called R, G, and B is projected. The intensities of the primary lights can be varied, while the relative spectral power distribution of each primary is constant. The observer's task is to adjust the intensities of the three primary lights so that the colors on the two sides of the bipartite field match, that is:

$$\mathbf{t} = R_t R + G_t G + B_t B \tag{2.2}$$

where the scalars R_t, G_t and B_t are called *tristimulus values* of $\mathbf{t}$.

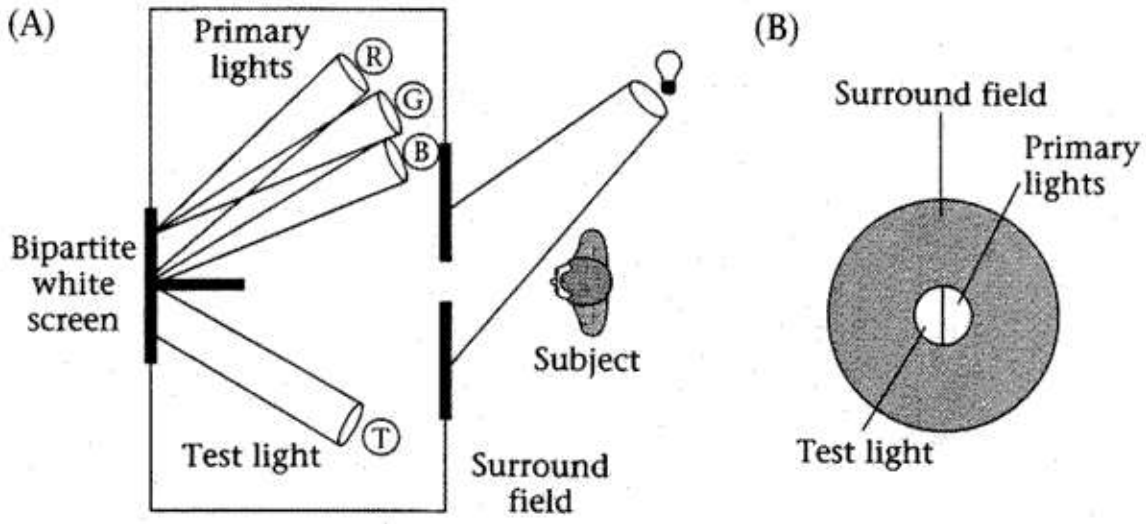

Figure 2.9: The color matching experiment. The observer views a bipartite field and adjusts the intensities of the three primary lights to match the appearance of the test light. (a) A top view of the experiment apparatus. (b) The appearance of the stimulus to the subject.

One can easily verify that photopic color-matching satisfies homogeneity and superposition, that is:

1. *Symmetry*: If color stimulus **A** matches color stimulus **B**, then color stimulus **B** matches color stimulus **A**.

2. *Transitivity*: If **A** matches **B** and **B** matches **C**, then **A** matches **C**.

3. *Proportionality*: If **A** matches **B** then $\alpha\mathbf{A}$ matches $\alpha\mathbf{B}$, where α is an arbitrary constant that changes the radiant power of the color stimulus while keeping its relative spectral distribution the same.

These empirical properties are called *Grassmann's laws of additive color mixtures* [19].

The color-matching experiment defines a linear mapping from the test light spectral power distribution to the intensity of the three primary lights. So there must be a $3\times n_\lambda$ system matrix $\mathbf{C}$ that maps the input $\mathbf{t}$ to the output $\mathbf{e}$: $\mathbf{e}=\mathbf{C}\mathbf{t}$. Thus, by matching a series of unit-intensity monochromatic lights, we can define each of the columns of the system matrix $\mathbf{C}$.

Each row of the matrix defines the intensity of a single primary light that was set to match the monochromatic test light. The rows of the system $\mathbf{C}$ are called *color-matching functions* (CMFs). Note that the color-matching functions are not unique, but each pair of color-matching functions will always be related by a linear transformation.

We must underline that such experiment is based on the principle of metamerism and, as a consequence of that, a match for one observer will probably not remain a match for another one. For that reason, an average observer, the *standard observer*, was introduced to replace any particular observer.

The 1931 CIE Standard Observer

The Colorimetry Committee of the CIE introduced in 1931 a set of color-matching functions for the standard observer based on the average results of 17 color-normal observers having matched each wavelength of the equal-energy spectrum with primaries of 435.8 nm, 546.1 nm and 700 nm. This set of color-matching functions is known as $\overline{r}_\lambda, \overline{g}_\lambda$ and $\overline{b}_\lambda$ (see fig. 2.10). This set of color-matching functions obtained by Guild [1] and by Wright [2], had anyway a great inconvenient: they feature both positive and negative values, which is not convenient from a practical point of view because it increases the complexity and the costs of the instruments needed to measure the tristimulus coordinates.

XYZ Color Space

For that reason, the same year the CIE defined the *standard system of color representation* shown in fig. 2.11.

This set of color-matching functions defines the *XYZ tristimulus coordinate system*; the color-matching functions in this system are called $\overline{x}_\lambda, \overline{y}_\lambda$ and $\overline{z}_\lambda$. This new set was chosen for several reasons. First, $\overline{y}_\lambda$ is a rough approximation of the brightness of monochromatic lights of equal size and duration, the *standard photopic luminosity function* $V(\lambda)$. Then, all the functions are nonnegative. One serious drawback of such a choice is that there is

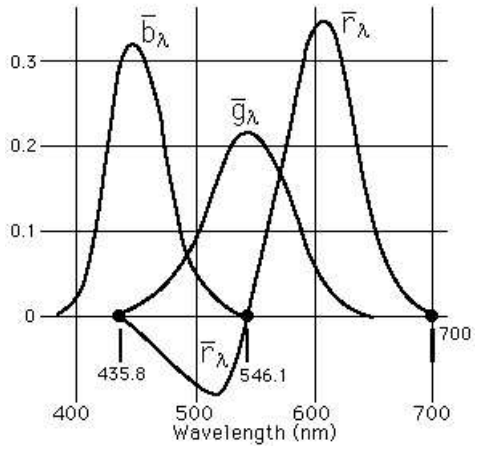

Figure 2.10: Color matching functions measured with monochromatic primary colors red (700 nm), green (546.1 nm) and blue (435.8 nm).

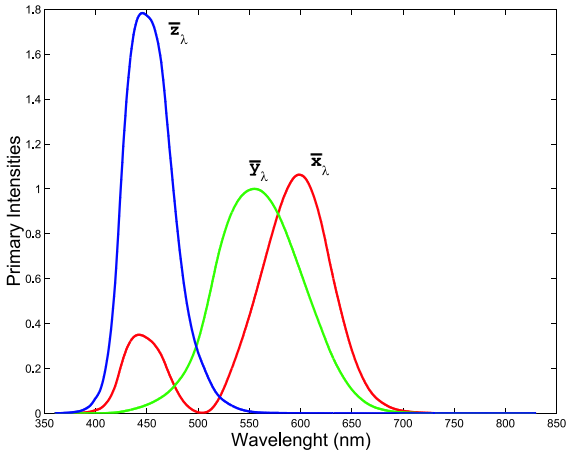

Figure 2.11: CIE 1931 standard color matching functions, based on the chromaticity coordinates obtained by Guild [1] and Wright [2].

no set of physically realizable primary lights that, by direct measurement, will yield the color-matching functions. Primary lights that would yield these functions would have to have negative energy at some wavelengths and can not be instrumented.

This set of color-matching functions is also referred to as the CIE 1931 2° CMFs [20] as they have been evaluated for the central 2° of visual angle. In 1959 Stiles and Burch [10] measured the most comprehensive set of CMF data in a "large field" 10° color-matching experiment. The results are the base for the CIE 1964 10° CMFs [21].

Some time later, it was discovered that the color matching functions adopted by CIE in 1931 are inaccurate. In particular, such curves underestimated the tristimulus values at

short wavelengths. In 1951, Judd [22] reconsidered the CIE 1931 standard. He discovered that the standard did not accurately reflect human color-matching performance. His analysis was later improved by Vos [23]. The Judd-Vos analysis produced a set of color matching functions (based on the same primaries as the CIE 1931) that are more typical for an average human observer than the CIE 1931 standard. The often cited Smith and Pokorny [24] cone sensitivity curves were obtained using the Judd-Vos color matching functions.

By means of the XYZ tristimulus values we can define the *chromaticity coordinates* *x,y,z*. It was observed that when the tristimulus values are scaled by the same factor, the stimulus becomes brighter but its "color" (hue and saturation) remains unchanged. Chromaticity coordinates, $\{x,y\}$, were therefore introduced so that hue and saturation can be specified independent of luminance. These coordinates correspond to the X and Y values normalized by the sum of the tristimulus values, that is:

$$x = \frac{X}{X+Y+Z} \quad \text{and} \quad y = \frac{Y}{X+Y+Z} \tag{2.3}$$

2.3.3 Opponent Modulation Color Spaces

To capture the essence of subsequent visual processing, color spaces based on the difference of responses rather then their absolute values were used by several researchers.

More Nearly Uniformly Spaced Systems: CIELAB and CIELUV Color Spaces

Chromaticity diagrams are very useful in colorimetry, but although the CIE *x,y* diagram has been widely used in the past, it does suffer from one important disadvantage.

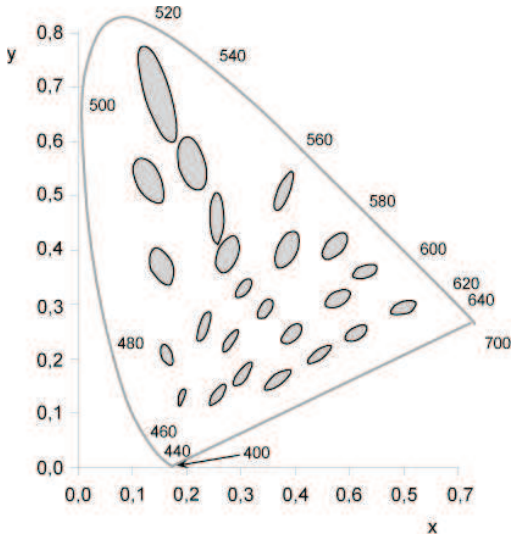

Figure 2.12: MacAdam's ellipses.

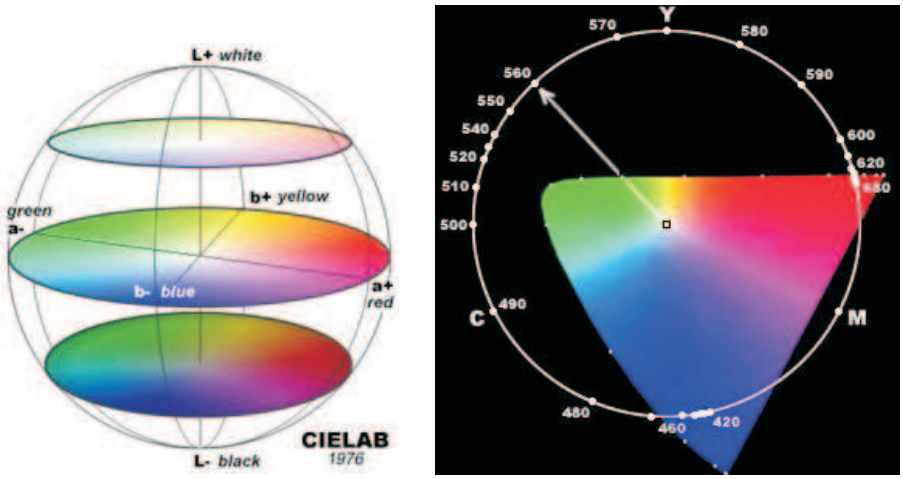

(a) (b)

Figure 2.13: Perceptual color spaces: (a) CIELAB (1976); (b) CIELUV (1976).

In fig. 2.12, areas are shown representing a constant perceptual color stimulus, at a constant luminance, at various positions and in various directions, in the $\{x,y\}$ diagram. It is clear that these distances vary greatly in length. This means that the XYZ color space (as the RGB color space) is not *perceptually uniform*. To avoid this nonuniformity, CIE recommended a new CIE 1964 *UCS (Uniform-Chromaticity Scale) diagram*, to be used with constant luminance levels. In 1976 the CIE defined two other color coordinate systems: the CIELUV ($L^*u^*v^*$) and the CIELAB ($L^*a^*b^*$) [25] (see fig. 2.13).

The CIE 1976 $L^*a^*b^*$ (CIELAB) color space is defined from the XYZ color space as follows:

$$\begin{aligned} L^* &= 116(Y/Y_n)^{1/3} - 16 \\ a^* &= 500[(X/X_n)^{1/3} - (Y/Y_n)^{1/3}] \\ b^* &= 200[(Y/Y_n)^{1/3} - (Z/Z_n)^{1/3}] \end{aligned} \tag{2.4}$$

for values of X/X_n, Y/Y_n and Z/Zn all grater or equal to 0.01, while for values smaller than 0.01, the previous relationship must be replaced by the following:

$$\begin{aligned} L^* &= 116\left[f\left(\frac{Y}{Y_n}\right) - \frac{16}{116}\right] \\ a^* &= 500\left[f\left(\frac{X}{X_n}\right) - f\left(\frac{Y}{Y_n}\right)\right] \\ b^* &= 200\left[f\left(\frac{Y}{Y_n}\right) - f\left(\frac{Z}{Z_n}\right)\right] \end{aligned} \tag{2.5}$$

where $f(Y/Y_n) = (Y/Y_n)^{1/3}$ for Y/Y_n greater than 0.008856, while, for Y/Y_n smaller than or equal to 0.008856, $f(Y/Y_n) = 7.787(Y/Y_n) + 16/116$; $f(X/X_n)$ and $f(Z/Z_n)$ similarly defined. Here X, Y and Z are the tristimulus values of the considered color while X_n, Y_n and Z_n are the tristimulus values of the reference white or light source.

Similarly, the equations for CIE 1976 $L^*u^*v^*$ (CIELUV) color space are:

$$\begin{aligned} L^* &= 116\left(\frac{Y}{Y_n}\right)^{1/3} - 16 \\ u^* &= 13L^*(u' - u'_n) \\ v^* &= 13L^*(v' - v'_n) \end{aligned} \tag{2.6}$$

where u' and v' are given by:

$$\begin{aligned} u' &= \frac{4X}{X + 15Y + 3Z} = \frac{4x}{-2 + 12y + 3} \\ v' &= \frac{9Y}{X + 15Y + 3Z} = \frac{9y}{-2x + 12y + 3} \end{aligned} \tag{2.7}$$

and u'_n and v'_n refer to the reference white or light source.

The transformations needed to map the CIE XYZ space to these two more perceptually uniform color spaces are thus nonlinear. This is somehow impractical but necessary, as linear color transformations do not generate natural and uniform color spaces.

Cone Contrast Space

The cone contrast space is based on the assumption that cone excitations are subsequently coded as contrast relative to some background signal; more precisely a Weber-style normalization is assumed.

Let L, M and S represent the excitations of the three cone types. Thus, the corresponding differential responses $\Delta L, \Delta M, \Delta S$ with respect to a background, producing an excitation on the three cone types of L_o, M_o and S_o respectively are:

$$\begin{bmatrix} \Delta L \\ \Delta M \\ \Delta S \end{bmatrix} = \begin{bmatrix} L - L_o \\ M - M_0 \\ S - S_0 \end{bmatrix} \tag{2.8}$$

DKL Color Space

The DKL color space was introduced by Derrington, Krauskopf and Lennie [26] in 1984 to characterize the output of the human vision opponent-color model. The axes of this color space, based on the MacLeod and Boynton [27] color diagram, are the three *cardinal directions* founded by Krauskopf et al. [4] using discrimination experiments. Around these

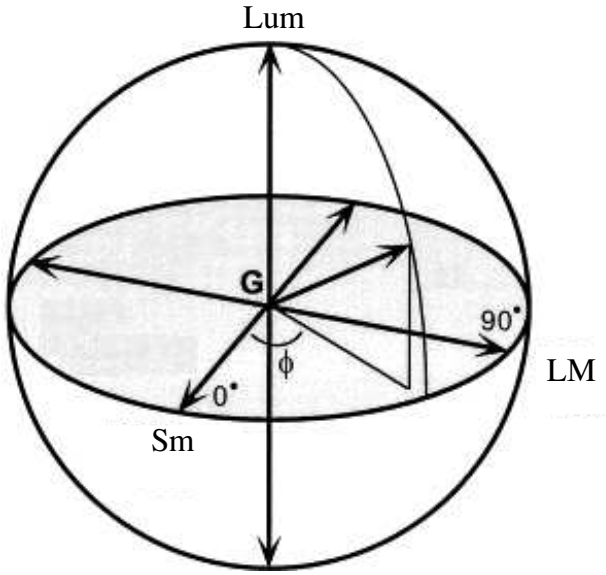

Figure 2.14: Color space of Derrington et al. (DKL).

directions Derrington et al. found three populations of cell types in the Lateral Geniculate Nucleus of primates.

The DKL color space (see fig. 2.14) is related to the LMS cone contrast space by a linear transformation, and like this one represents the differential responses (with respect to some background signal), rather than the absolute responses of the different color channels. The axes represent approximately the differential outputs of the achromatic (ΔLum), the red-green (ΔLM) and the yellow-blue (ΔSm) mechanisms. The relation between the cone contrast space and the DKL color space can be easily defined assuming that the following properties hold between the differential cone excitations (ΔL, ΔM, ΔS) and the outputs of the three channels:

- The output of the achromatic mechanism ΔLum is proportional to the sum of the differential output of L and M cones (ΔL and ΔM), and receives no input from S cones (i.e. S-cone excitation does not influence luminance).

- The red-green and yellow-blue mechanisms produce zero differential response when the considered signal has the same chromaticity as the background signal (these mechanisms are chromatic mechanisms).

- The red-green channel receives no input from the S cones.

- The yellow-blue mechanism response ΔSm is zero if both the differential S-cone excitation and the differential response of the achromatic mechanism are zero.

Then, the following relationship holds:

$$\begin{bmatrix} k_{Lum}\Delta Lum \\ k_{LM}\Delta LM \\ k_{Sm}\Delta Sm \end{bmatrix} = \begin{bmatrix} 1 & 1 & 0 \\ 1 & -L_0/M_0 & 0 \\ -1 & -1 & (L_0+M_0)/S_0 \end{bmatrix} \begin{bmatrix} \Delta L \\ \Delta M \\ \Delta S \end{bmatrix} \tag{2.9}$$

where L_0, M_0 and S_0 are the coordinates of the background color in the LMS space. Note that the coefficients of the transformation matrix for the color channels vary with the background. The constants k_i define the units for the mechanism response. Setting the k_i constants means defining a color contrast metric. A natural choice for k_{Lum} is to set it so that ΔLum represents the luminance contrast. For the other two constants there is not such a natural choice. The most convenient strategy seems to be setting k_{LM} and k_{Sm} so that each mechanism has a unit response when excited in isolation by a stimulus with unit *pooled cone contrast* (pooled cone contrast $= \sqrt{(\Delta L/L_0)^2 + (\Delta M/M_0)^2 + (\Delta S/S_0)^2}$). This choice, proposed by Brainard [28], is the one we decided to adopt. In this way we obtain:

$$\begin{aligned} k_{Lum} &= \frac{L_0+M_0}{\sqrt{L_0^2+M_0^2+S_0^2}} \\ k_{LM} &= \frac{L_0+M_0}{\sqrt{2}M_0} \\ k_{Sm} &= \frac{L_0+M_0}{S_0} \end{aligned} \tag{2.10}$$

The DKL color space is the color space we are going to use to define our experiment. This because it explicitly represents the responses of retinal processing, facilitating the characterization of post-receptoral mechanisms.

2.4 Conclusions

In the first part of the chapter, the physiology of the human eye, the retina and the visual cortex were described. These are the main elements of the human visual system and for an understanding of its abilities, the knowledge of the physiological structures is necessary. The optics of the eye were illustrated and it was discussed how the different elements of the human eye can influence color perception. A detailed description of the various retina layers offered an insight into the first levels of visual processing in the HVS. The complete way of visual information, from the photoreceptors to visual cortex, through the visual pathways, has been described.

In the second part of the chapter, we have introduced the science of color specifying, the colorimetry. We have described the classical color-matching experiments, based on the basic Grassmann's law of additive color mixtures, and the color systems based on color-matching tests like the XYZ color space. More perceptive color spaces like the CIELAB

and the CIELUV have been exposed. In the final part of the section, opponent modulation color spaces have been presented. The DKL color space has been described in detail, being the one we have used to draw the stimuli for our experiment.

The next chapter will describe the main color vision mechanisms, starting from the basic phenomena. These effects are of great importance for understanding the behavior of HVS, and have to be known before approaching the higher order color mechanisms. Moreover, these phenomena affect the performance of the visual system and have to be accurately considered before setting a psychophysical experiment.

Chapter 3

Color Vision Mechanisms

3.1 Introduction

The perception of a chromatic pattern can be influenced by a great number of factors. Spatial and temporal characteristics of a stimulus, size, illumination, geometry, play a fundamental role in color perception.

In this chapter we describe a number of psychophysical low- and high-level vision effects. Low-level vision effects are characterized by a quite simple behavior and can usually be easily modelled. High-level vision phenomena, on the other hand, are much more complex and far to be understood and integrated into a HSV model. They need, nevertheless, to be respected for a correct setup of a psychophysical test.

In the final part of the chapter, we introduce some basic concepts of psychophysics in order to show the key role of psychophysical experiments in the development of human visual system knowledge. Then, the higher order color mechanisms are introduced and a review of the most significant studies on the subject is presented. The higher order color mechanisms represent the way the brain process the chromatic information coming from the eye through the opponent channels. The gaol of the section is to clarify the concept of higher order mechanism and to show the work of D'Zmura and Knoblauch [3] that has inspired the presented subject.

3.2 Low-Level Vision Phenomena

The opponent mechanisms described in chapter 2 operate at the level of the retina, where the cones combine to form the opponent signals. The information brought by the three opponent channels is then further processed by the brain. The existence of *higher order* mechanisms responsible for color vision has emerged on a phenomenological basis, to account for phenomena affecting color perception for which a physiological ground has still to be identified.

3.2.1 Weber-Fechner Law

In the nineteenth century, E. H. Weber investigated the perception of heaviness of lifted weights His law is mainly founded on experiments where persons were given two nearly identical stimuli (in his particular case, two similar weights) and tested whether they could notice a difference between them. It was found that the smallest noticeable difference was roughly proportional to the intensity of the stimulus. For example, if a person could consistently feel that a 110 g weight was heavier than a 100 g weight, in the same way, he could feel that 1100 g was more than 1000 g.

If the initial magnitude of the stimulus is denoted by I and the change required to achieve a threshold is denoted by ΔI, Weber's results can be expressed by stating that the ratio $\Delta I/I$ is constant at threshold. This relationship holds approximately true for many perceptual stimuli and has come to be known as the Weber's law.

Based on such an observation and exploiting the fact that a constant relative difference in the intensity corresponds to a constant absolute difference in the logarithm of the intensity, in 1860, Fechner [29] suggested that the *perceived* magnitude R is proportional to the logarithm of the stimulus intensity S:

$$R = k \log \left(\frac{S}{S_0} \right) \tag{3.1}$$

where k and S_0 are constants. This formula is widely known as the Weber-Fechner law.

If Weber-Fechner law were strictly valid, then the relationship would follow the same form for every kind of perception. Whereas, it was noticed that various perceptions take on relationships with differently shaped functions. The Weber-Fechner law is not completely accurate.

3.2.2 Stevens' Law

In 1961 Stevens [30] published a paper where he studied the relationship between the intensity of a physical stimulus and its perceptual magnitude for over 30 different types of perceptions using a magnitude estimation technique. He found that the results from different sensory modalities varied too much in ""steepness" to be fitted by the Weber-Fechner law. Instead, he proposed a different model with an additional parameter, α:

$$R = k(S - S_0)^{\alpha} \tag{3.2}$$

If we take the logarithm of both sides of this formula, we get:

$$\log R = \alpha(S - S_0) + \log k \tag{3.3}$$

That is, a linear relationship is established between $\log(S - S_0)$ and $\log R$, α being the slope of the line. This type of data are naturally presented in bilogarithmic diagrams, as shown in fig. 3.1.

For the perceived brightness/lightness, the power law in the form:

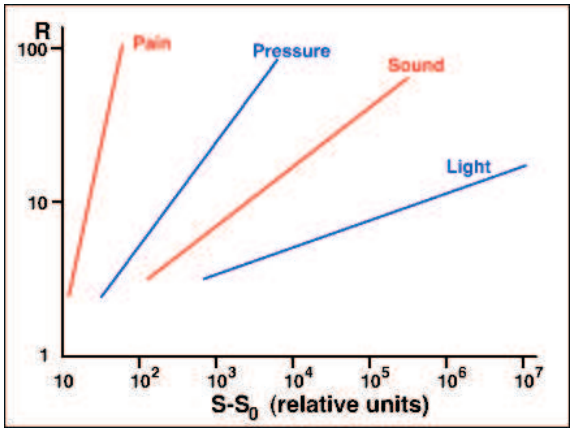

Figure 3.1: Various psychophysical response functions.

$$B = k_l L^{\alpha_l} + B_0 \tag{3.4}$$

is found to be the preferred description [31], where B indicates the brightness/lightness estimated by the observer for a stimulus with given luminance L and B_0 is a constant offset of perceived brightness/lightness. The exponent α_l has a value of approximately 1/3: the power law with an exponent of 1/3 is also part of the color space $L^*a^*b^*$.

3.2.3 Contrast Sensitivity Function

The appearance of a colored stimulus, as is the case for graylevel patterns, depends on its spatial and temporal frequency. The three opponent channels have different spatial resolutions: this is of great importance in applications such as broadcast television and digital color imaging.

The characteristics of the HVS from the temporal and spatial point of view are defined by the *Contrast Sensitivity Function* (CSF). CSFs are typically measured by presenting to an observer a temporal or spatial sinusoidally varying stimulus. The contrast of the target is then varied and the observer's contrast detection threshold is determined. Since high levels of visual sensitivity, for temporal or spatial variations, correspond to low contrast thresholds, a reciprocal measure (1/threshold), the *sensitivity score*, is used. The contrast sensitivity scores obtained for each of the stimuli are then plotted as a function of the target spatial or temporal frequency.

Contrast is usually defined as the maximum luminance minus the minimum luminance present in the stimulus divided by their sum:

$$C = \frac{L_{max} - L_{min}}{L_{max} + L_{min}} \tag{3.5}$$

The image in fig. 3.2 is a nice example of such a phenomenon. The luminance of peaks and troughs remains constant along any horizontal line through the image. Therefore, if

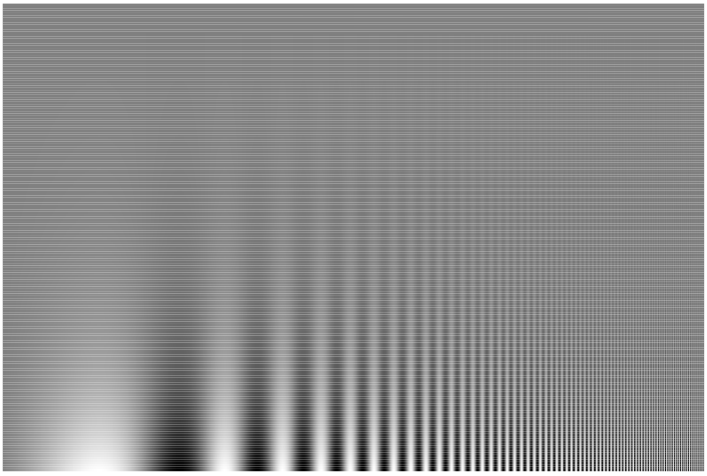

Figure 3.2: Modulated sine wave grating. The observer can see his/her own luminance CSF.

the detection of contrast were dictated solely by image contrast, the alternating bright and dark bars should appear to have equal height everywhere in the image. However, the bars appear taller in the middle of the image than at the sides. This inverted-U shaped envelope of visibility is *your* contrast sensitivity function. The exact location of the peak depends on the viewing distance.

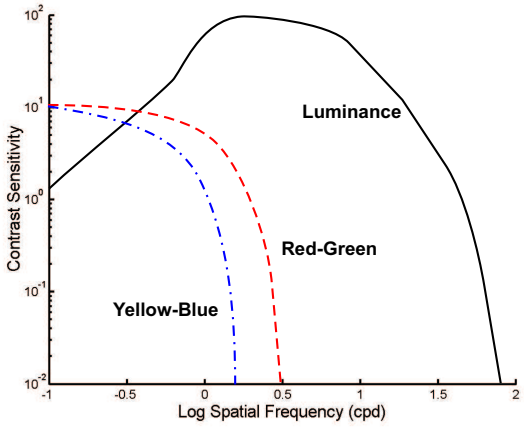

Figure 3.3: Spatial contrast sensitivity functions for luminance and chromatic contrast.

As shown in fig. 3.3, spatial CSF for luminance contrast is band-pass in nature, with a peak sensitivity around 5 cycles per degree [12]. This function approaches zero at zero cycles per degree, illustrating the tendency for the visual system to be insensitive to uniform fields. It also approaches zero at about 60 cycles per degree, the point at which details

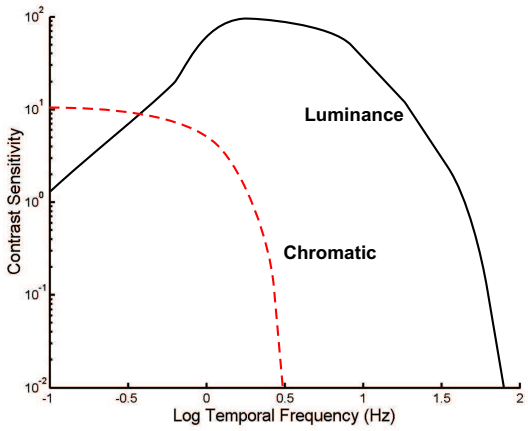

Figure 3.4: Temporal contrast sensitivity functions for luminance and chromatic contrast.

can no longer be resolved by the human eye. The chromatic mechanisms are of a low-pass nature and have significantly lower cut-off frequencies. This indicates the reduced availability of chromatic information for fine details. The yellow-blue CSF has a lower cut-off frequency then does the red-green one, because of the small number of S cones in the retina. Note also that the luminance CSF is much higher than the chromatic CSFs. This denotes a greater sensitivity in the visual system to small changes in luminance contrast compared to chromatic contrast.

Typical temporal CSFs for luminance and chromatic contrast are shown in fig. 3.4 [12]. They share many characteristics with the spatial CSFs shown in fig. 3.4. Luminance temporal CSF is still higher in both sensitivity and cut-off frequency than are the chromatic temporal CSFs. It also exhibits band-pass characteristics, while chromatic temporal CSFs have low-pass behavior.

3.2.4 Adaptation Mechanisms

In this paragraph we consider the dynamic mechanisms of adaptation that serve to optimize the visual response to the particular viewing environment.

DARK ADAPTATION Coming from a very bright area to a dim one, everyone can experience how difficult it is to see for several minutes just after having come indoors. This phenomenon is called *dark adaptation*. It is due to the change in visual sensitivity that occurs when the prevailing level of illumination decreases.

Fig. 3.5 shows the course of visual sensitivity after transition from an high illumination level to complete darkness [32]. At first, the cones become more sensitive. Then, after about 10 minutes, the rods, which have a longer recovery time, have recovered enough sensitivity to outperform the cones and thus begin controlling overall sensitivity.

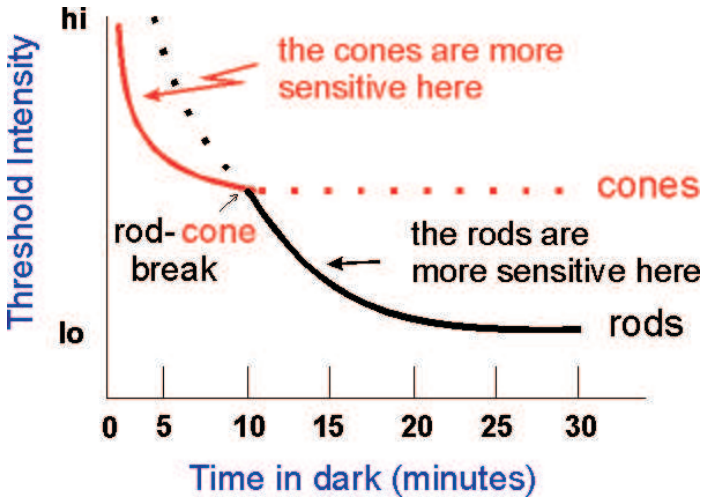

Figure 3.5: Dark adaptation curve showing the recovery of threshold intensity after transition from an high illumination level to complete darkness.

LIGHT ADAPTATION *Light adaptation* is essentially the inverse process of dark adaptation. It occurs when one goes from a dark environment to a bright one. Thus, the visual system must become less sensitive, since there is much more energy available.

One of the major differences between dark adaptation and light adaptation is their time course. Whereas dark adaptation takes about 30 minutes to be complete, light adaptation happens very quickly, usually in less than a minute.

Another difference between these two types of adaptation is that when you are light adapted and then go into a very dark room for a while you may not see anything at all. As you dark adapt more and more things become visible. When you go from a darker area to a very bright one you usually are not temporarily blind. It is just that your vision temporarily is not very good. In fact, your contrast sensitivity is poor until you become light adapted. That means that you will have some difficulty in perceiving areas of low contrast. But as you quickly light adapt, the darker areas become darker and the lighter areas become easier to see.

CHROMATIC ADAPTATION *Chromatic adaptation* is closely related to dark and light adaptation. In fact, similar physiological mechanisms are thought to produce these phenomena, which can be interpreted as an automatic white balance mechanism [12]. If the new lighting situation has a different color *temperature*, for example there is an increased amount of red light relative to the total amount of light, then the cells responsible for sensing red radiation will reduce their sensitivity relative to the sensitivity of the other cells. As a result, a white surface will again appear white to the observer after a certain time, although it reflects a proportionally increased amount of red light.

Another example of chromatic adaptation is *afterimages*. The colors in the afterimages are the result of sensitivity changes of the different chromatic mechanisms. For example,

retinal areas exposed to a red light become less sensitive to red energy during the adapting exposure, thus resulting in a cyan afterimage.

3.3 High-Level Vision Phenomena

3.3.1 Simultaneous Contrast

Simultaneous contrast causes a stimulus to shift in color appearance when the color of its background is changed. This apparent color shift follows the opponent-color theory in a contrasting sense along the opponent direction. This means that a light background induces a stimulus to appear darker, red induces green, yellow induces blue and so on. Fig. 3.6 shows an example of simultaneous contrast.

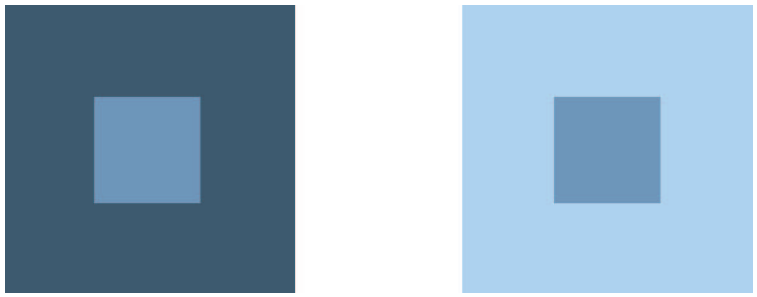

Figure 3.6: An example of simultaneous contrast. The central patches are physically identical.

Fig. 3.7 shows the complex spatial nature of this phenomenon. The light blue squares in the figure are identical and surrounded by the same chromatic edges. In spite of that, the color of the squares falling on the green stripes seems darker than that of the squares falling on the blue one. Clearly, the spatial structure of the figure plays a central role in the simultaneous contrast phenomenon.

3.3.2 Spreading

When the spatial frequency of the stimulus increases or decreases, the simultaneous contrast effect disappears and is replaced by a *spreading effect*. This effect is the apparent mixture of a color stimulus with its surround. However, spreading occurs at spatial frequencies above those at which fusion occurs. Thus, while the stimulus is still viewed as distinct from the background, their colors begin to blend.

Fig. 3.8 shows both simultaneous contrast and spreading. The two sets of gray patches occupy the same area on the light red background. Notice that the patches on the left appear slightly greenish. On the right, the gray patches definitely tend towards red. Simultaneous contrast is taking place on the larger blocks of the neutral gray. Whereas, the thinner strips of gray exhibit the spreading effect.

Figure 3.7: Stimulus illustrating the complexity of simultaneous contrast. The local contrasts for the left and right sets of square are identical, but the perceived colors are different.

Figure 3.8: Demonstration of the spreading effect compared with the simultaneous contrast phenomenon.

3.3.3 Color Constancy

Color Constancy is a widely discussed phenomenon. It is typically defined as the ability of the visual system to assign a color description to an object such that it does not depend on the illumination environment, allowing the system to recognize objects under many different illumination conditions. This mechanism is served by the mechanisms of chromatic adaptation and *color memory*. The latter is the phenomenon that associates prototypical colors with recognizable objects.

The phenomenon of color constancy allows observers to perceive the colors of objects independently of changes in illumination. Psychophysical experiments with human subjects have shown that although human color constancy is quite good, it is far from being perfect [33]. It also performs poorly in lighting with abnormal spectral content (i.e., sodium arc, or early fluorescents). However, it is an important tool in color vision related tasks.

3.4 Investigating Higher Order Color Mechanisms

After this quick, and inevitably incomplete, review of the most important and basic aspects of human color vision, we want now to focus our attention on the subject of this dissertation: the *higher order color detection mechanisms*.

The perception of spatial distributions of colors - simple two-color stimuli, textures or natural images - has been studied to try to understand the great number of mechanisms that such an experience involves. In fact, when looking at a colored scene, lots of mechanisms operating at a post-receptoral level are involved. Despite color vision is intensively studied, such mechanisms are still far to be satisfactorily explained, which makes them a very appealing subject.

3.4.1 Introduction

It is well known that a perceived color depends on the relationship between light signals from both that point and the surrounding area. In classical studies on *simultaneous color contrast* it was observed that objects acquire hues and brightnesses complementary to hues and brightnesses of the surrounds [13, 34, 35]. These shifts in color appearance provide a mechanism for *color constancy*, since contrasts in scenes remain relatively constant when the illumination changes, as already discussed in sec. 3.3. Simultaneous color contrast has been extensively investigated in classical color-vision texts (we refer to [36–39] for more complete analysis).

Color contrast has been generally studied using a test spot within an homogeneous surround, even though natural conditions for color vision are quite different and involve more complex surrounds and consequently more numerous and complex mechanisms. In 1905, Von Kries [40] hypothesized that a uniform background influences the appearance of a certain color by altering photoreceptoral sensitivity. His ideas are interpreted in terms of a simple multiplicative chromatic-adaptation model, acting independently within each cone class. This model is still one of the most satisfying, even if color-appearance studies since Von Kries have not decisively proved his hypothesis.

Even if contrast with respect to the immediate background has a huge influence on color appearance [41], this is not sufficient to explain how the color of an object is perceived in more natural viewing conditions. In fact, the influence of remote chromatic elements on the perception of colors has been reported by Hurvich [42] and Walraven [43], that found a distance-independent induction effect. Effects of chromatic context are strongly different from changes in appearance due to immediate chromatic contrast [44]. It has been observed that the main effect of remote chromatic contrast is not directly on the test field, but rather on the magnitude of the induction from the immediate surround on the test [44–46]. Wachtler et al. [46] also found that the induction effect produced by distant chromatic background depends on its contrast (see also [47]) while its effect is little when there is no chromatic contrast between the test and the immediate surround, confirming the findings of Shevell and Wei [45]. The importance of the variation within a stimulus in determining its appearance has been underlined by several recent studies. In a paper,

Jeness and Shevell [48] showed how even a very sparse chromatic information can alter the perception of a test light. Brown and MacLeod [49] show that color appearance is very strongly influenced by the *variance* of the surround colors, even if the spatial averaged mean luminance and chroma are the same.

As can be seen, a great number of visual phenomena are observed, but most of them are difficult to understand and to model. Perhaps this happens because we are not able to determine which are the basic components of the human visual system and their characteristics. The visual system uses a number of attributes in everyday vision tasks, such as spatial configuration, depth, color and luminance.

Starting from the inspiring work of Knoblauch and D'Zmura [3], we have set up a *psychophysical experiment* to investigate the higher order mechanisms underlying the perception of spatial distributions of colors.

3.4.2 Psychophysics

Psychophysical experiments have produced most of the knowledge we have of human visual system and visual phenomena. *Psychophysics* is the science of relating the physical measurements of stimuli with the sensations and perceptions that those stimuli provoke. Except for physiological, intrusive techniques, employed in medical researches, psychophysical techniques are the only ones suitable for the investigation of all the dimensions of human perception.

Psychophysical experiments are used to extract quantitative data from perceptual experiences, that are subjective. However, if a psychophysical experiment is properly designed and controlled, it could be as objective and precise as any other physical measurement. Even if the uncertainties of psychophysical measurements tend to be larger than those of physical tests, the results are equally useful and significant, as long as those uncertainties are pondered [12].

THRESHOLD EXPERIMENT In the presented work, a visual experiment is set up. In order to characterize the human color contrast detection mechanisms, we use a *threshold experiment*, which is particularly appropriate to measure the detectability of a stimulus [12]. In fact, with such experiments one can measure the just-perceptible change in a stimulus and thus estimate a detection threshold for that stimulus. The inverse of threshold is referred to as *sensitivity*, since low thresholds require high sensitivities.

A *two alternative forced choice* method (2AFC) is used to compute thresholds. The signal is presented in one of two intervals, that are spatially separated. The subjects are asked to indicate in which of the two intervals the signal was displayed. If they cannot detect it, they have to guess one of two intervals. This method is employed to limit the influence of varying observer criteria on the results, since observers cannot respond if they detect the signal, but they have just to indicate *where* the signal is displayed [12].

The 2AFC method is implemented with a *staircase procedure*. The observer's responses are controlled for each stimulus. If the subject detects the signal, the same signal level is presented, if they do not, the intensity of the signal is increased for the following trial.

The signal level is decreased after three consecutive correct answers. This method quickly *converges* about a value and present the advantage that a complete increasing or decreasing sequence is not presented, limiting adaptation and expectation errors [50].

THE PROCESS In order to properly set up a psychophysical test, one should plan a strict protocol that governs the experiment. This protocol is required to cover as many factors affecting the results of the threshold test as possible.

The process of setting up a psychophysical test consists of six basic steps [50]:

1. *Select the samples.* One should plan the size of the samples, their spatial and temporal frequencies and the range of values to be represented. All these aspects will be discussed in the next chapter.

2. *Prepare the samples.* The number of samples to be presented is a very important factor. It should be big enough to allow an accurate convergence of the staircase, but not so much to induce the observers to lose interest and hurry. In our experiment, we have used 48 stimuli for each staircase, that takes about 2 minutes to be completed.

3. *Select observers.* Observers with normal color vision have been selected. The number of observers is another key factor for the development of a psychophysical test. A large number of observers should give more precise results. In our study, we employ six observers.

4. *Determine observer task.* The task instructions should be clear and should communicate what exactly is the judgement task. Precise written task instructions are presented to the observers to read before the experiment.

5. *Present samples to observers for the experiment.* The principal variables to be considered are the viewing conditions and the mode of presentation. We present our stimuli in a completely dark room. The stimuli are displayed within a neutral grey background that provides a constant visual reference. The viewing distance is fixed to 50 cm. One should also consider environmental factors, such as psychological and physical comfort, noise and surround that could distract the observers. Subjects take pauses every about ten minutes to relax, and the most comfortable viewing position is chosen by each observer.

6. *Conducting the psychophysical test* As already discussed in that section, a staircase procedure is used to estimate the thresholds. Small-size trials are effected to test and debug the experiment protocol and to set up the psychophysical test.

All these aspects have been carefully considered and analyzed in order to perform a reliable psychophysical experiment and to control as many sources of uncertainty as possible.

3.4.3 Higher Order Mechanisms: State of the Art

As already discussed in chapter 2, there is general agreement on the fact that color information is processed by hierarchical mechanisms: the signals from three types of cone receptors each with its own photopigment at the first stage are linearly combined to form three cone-opponent channels at the second level. The interactive nature of this second stage is widely accepted and is supported, as we have already seen, by many psychophysical experiments. In addition, a great number of physiological works have shown that signals from different types of cone photoreceptors are combined in an opponent fashion. From that level, the behavior of the human visual system concerning the treatment of color information is much disputed and far to be exhaustively understood.

Results of psychophysical chromatic detection experiments have typically been interpreted in terms of red-green (R-G) and yellow-blue (Y-B) detection mechanism combined with a non-opponent luminance mechanism. Recently, the classical notion of chromatic information encoded by the visual system along opponent channels, has been debated by reports of psychophysical works showing the evidence for chromatic mechanisms tuned to specific directions in the color space [3–8].

Krauskopf et al. [4,5] used an habituation experiment to determine the so-called *cardinal directions* of color space. Signals varying along these axes are carried along separate, post-receptoral mechanisms. They measured the detection thresholds for a 2° circular field before and after exposure to sinusoidal variation in chromaticity along cardinal and intermediate directions. It was observed that thresholds for detecting changes in color are raised after viewing the modulated field. Moreover, it was observed that this phenomenon is highly selective. For example, thresholds for detecting red and green changes from white are raised after viewing a field modulated in the red-green direction, but not after viewing a field varying in a yellow-blue direction. In 1986, they reported that the elevation of thresholds, caused by pre-exposure to these modulations of chromaticity along an intermediate color direction in the isoluminant plane, was minimal for color contrast signals along the perpendicular axis. This phenomenon suggested the presence of detection mechanisms sensitive to specific hues in the color plane. Krauskopf et al. called these mechanisms *higher order color mechanisms*, beyond the previously identified second stage, opponent, mechanisms.

Webster and Mollon [8] extended the threshold adaptation paradigm of Krauskopf et al. [4] to suprathreshold color appearance. They found that adaptation changed the perceived color of chromatic test fields reducing their saturation and changing their hue. This effect was observed to be very selective, consistent with channels selectively tuned to any color-luminance direction. Still working at suprathreshold levels, D'Zmura [6] found evidence of higher order color mechanisms with a visual search experiment.

Gegenfurtner and Kiper [7] measured detection thresholds for small gratings within broadband masking noise. Signal and noise were modulated along different directions in color space. They observed that a linear relationship between signal and noise hold while they were modulated along the same axis, while no masking effect was noticed when signal and noise were lying on different directions.

Thus, results of many kinds of psychophysical works strongly suggest the existence of color detection mechanisms with spectral sensitivities tuned to a variety of directions in the color space. Nevertheless, a general agreement is still far from being reached.

In their work with chromatic masking in (ΔL/L, ΔM/M) plane of cone contrast space, later extended to the DKL equiluminant plane, Giulianini and Eskew [51, 52] found no evidence of higher order chromatic mechanisms. In fact, in their masking experiment with Gaussian and Gabor patches they did not observe a maximal elevation of the threshold when the masking noise was added along the direction of the signal. These results suggested that the activity of only three mechanisms mediate the detection: the achromatic mechanism (L + M) together with the two opponent chromatic mechanisms (L - M) and (S - L - M).

Physiological research is still not able to put an end to this discussion. However, results of electro-physiological experiments on neurons of macaque monkeys seem to suggest the existence of such higher order mechanisms. While the spectral sensitivities of neurons in lateral geniculate nucleus (LGN) tend to be oriented along two main directions in the achromatic plane [26, 53], neurons in cortical areas V1, V2 and V3 have been found with spectral sensitivities oriented along many different directions in the color plane [54–57]. In the visual cortex, color-sensitive neurons have been observed that are most sensitive to hues lying *between* the main directions that characterize retinogeniculate processing.

Another interesting open issue is about the behavior of these color detection mechanisms and more precisely about their spectral sensitivity. Have chromatic mechanisms broad or narrow spectral sensitivities? Broad spectral sensitivity is coherent with the hypothesis of linear combination of cone signals, while narrow sensitivity could result only from a non-linear combination of the photoreceptors signals. From physiological studies, it is known that a large number of color sensitive neurons combine cone photoreceptor signals linearly [26, 54]. On the other hand, cortical neurons in areas V1 and V2 with narrowly-tuned spectral sensitivities have been found [54, 56].

The questions about higher order color mechanisms and their characteristics have been faced by Knoblauch and D'Zmura [3] in a study of 1998. In the next section, we describe accurately their study, that have inspired the presented work, and the techniques they have developed.

3.4.4 The Paradigm of K. Knoblauch and M. D'Zmura (1998)

D'Zmura and Knoblauch [3] investigated the problem of the existence of higher order color mechanisms and their nature via a noise masking technique. They estimated the color detection thresholds for three observers using a sectored noise masking technique, in an equiluminant plane of the DKL color space (see sec. 2.3.3). Sectored noise chromaticities were randomly sampled from a sector of variable width in the color plane, oriented along the same direction $\overrightarrow{a}$ of the signal (see fig. 3.9). The amplitude n and the half width θ of the sector were under experimental control.

This interesting technique induces the observers to use a single color detection mechanism and allows an estimate of the spectral bandwidth of such mechanisms by varying

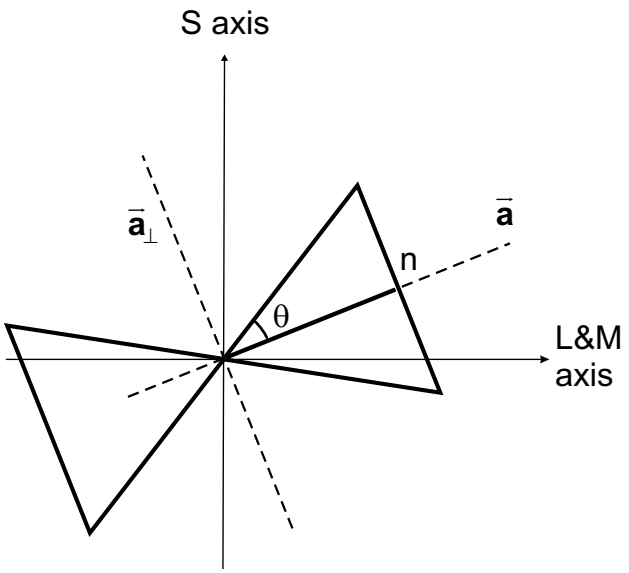

Figure 3.9: Sectored noise of amplitude n and half width θ, oriented along the direction $\overrightarrow{a}$.

the width of the sector. In fact, measuring the efficacy of noise masking as a function of sector width, it is possible to distinguish between detection mechanisms that combine the cone inputs linearly and mechanisms that combine the cone signals in a nonlinear fashion. In fact, since a linear mechanism tuned to a certain direction $\overrightarrow{a}$ of the color space can be represented as a vector in the DKL space, the response of such a mechanism to a stimulus is given by the dot product between those two vectors representing the mechanism and the stimulation. Thus, the noise components orthogonal to the mechanism direction do not affect the mechanism behavior itself. Varying the noise sector width one can vary only the noise components orthogonal to the test signal direction, and thus to the vector representing the detection mechanism. Thus, the performances of a linear detection mechanism are not influenced by a variation of the noise sector width. On the other hand, if a non linear mechanism mediates the detection, noise masking efficacy is expected to vary when noise sector width varies.

In their experiment, D'Zmura and Knoblauch showed to their subjects a large colored Gaussian spot with a space constant of about 2.4° of visual angle, displayed on a uniform gray background. Temporal and chromatic properties of the stimulus (signal plus noise mask) are diagrammed in fig. 3.10, directly drawn from the original paper. The chromaticity of the stimulus was a temporal modulation of the chromaticity of the signal summed to that of the sectored noise. Thus, the signal had a gaussian time-course with a duration of 640 ms and was the result of a mono-polar modulation along a chromatic axis from the reference gray point. The noise was a rapid, time-varying modulation of the chromaticity of the Gaussian patch with a time frequency of 100 Hz.

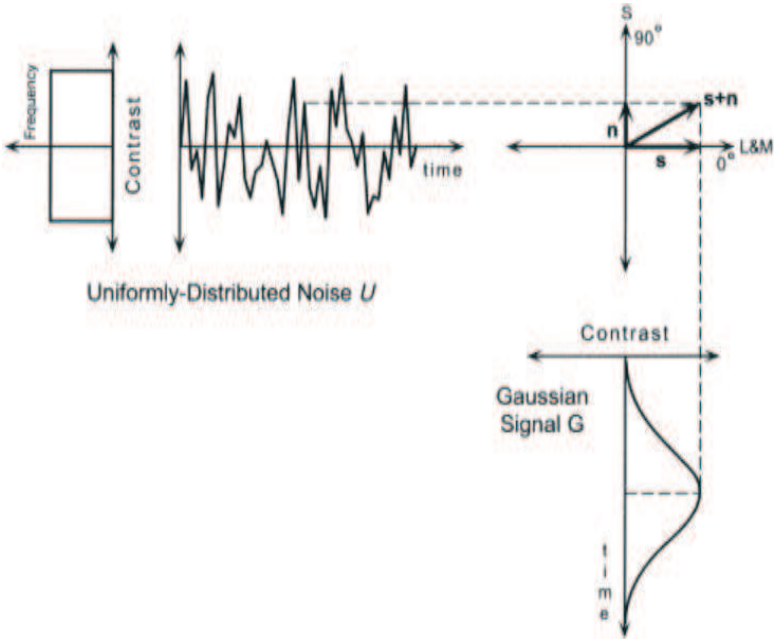

Figure 3.10: Combination of signal and axial noise using vector addition. Signals (bottom right) are presented with a Gaussian time-course and may vary in the chromatic axis along which they are presented and in their peak contrast. Shown is an equiluminant signal along the *red* limb of the L and M cone axis (see equiluminant plane at top right). Axial noise samples (top left) are drawn 100 times/s from a uniform density with a maximum contrast under experimental control. The samples are used to modulate chromaticity along an arbitrary chromatic axis; shown is noise along the S cone axis. At any time t the signal $s(t)$ is added to the noise $n(t)$ to generate the instantaneous modulation of chromaticity. The vector addition of signal and noise is shown at the time of the signal peak.

The results of the experiments for detection of yellow, red, orange and violet signals showed a substantial independence of the masking effect on noise sector width. Thus, the most plausible way to account for their results was to derive that the human visual system uses linear higher order detection mechanisms tuned to the set of tested color axes. As expected, two of these directions coincide with the two chromatic cardinal mechanisms, namely the red and the yellow. The same trend was observed for the other intermediate directions in the color plane, suggesting that, consistently with the initial guess, there exist detection mechanisms tuned to a variety of directions in the chromatic space that combine the cone photoreceptors inputs in a linear fashion.

In this project, we extend the methods used by K. Knoblauch and M. D'Zmura to the *spatial domain* to investigate higher order mechanisms that take part in the perception of spatial distributions of chromatic elements.

3.5 Conclusions

In this chapter, we have exposed the main color vision mechanisms. In the first sections we have shown some visual phenomena involved in human vision. The knowledge of the basic phenomena, such as contrast sensitivity and adaptation, is of crucial importance for a correct understanding of the human visual system. Moreover, some high-level vision phenomena have been exposed. These effects, even if far to be completely understood, have to be considered when designing a psychophysical experience, because they strongly affect vision performances.

In the last sections, higher order color mechanisms have been introduced. They can be seen as a way to model how the human brain process the visual information. We have also introduced some basic concepts of psychophysics. The most important studies on the domain of higher order mechanisms have been reviewed, with particular attention to the work of D'Zmura and Knoblauch, that have inspired the presented project.

Chapter 4

Methods and Experiments

4.1 Introduction

How colors are perceived and which mechanisms control human color vision are still open issues. In the present work we particularly focus our attention on the color detection mechanisms operating in spatial color vision.

In that chapter, the experiment that was set up to investigate color detection mechanisms is described in detail. In section 2 the basic ideas underlying the experiment are exposed. Section 3 resumes the DKL color space, which is used to define the stimulus. A description of the creation of the stimulus, e.g. signal and noise, is provided in section 5. In particular, the sectored noise masking technique is analyzed and explained. In sections 7, the protocol of the experiment is exposed while in section 8 the apparatus that was used and its calibration and characterization are described.

4.2 The Idea

Among the main open issues in the field of color perception, we focus on the following:

- *Which are the detection mechanisms involved in the perception of chromatic spatial patterns?*
- *Which are the characteristics of these mechanisms?*

As discussed in Chapter 3, three main mechanisms operate at the retina level, the achromatic, the red-green and the yellow-blue. These basic mechanisms, known as opponent color channels, contribute to everyday visual detection tasks. One aspect we are going to investigate is whether there are mechanisms for the detection of color whose spectral sensitivities lie between those of the three principal one. Psychophysical and physiological studies suggest that such "intermediate"" mechanisms exist [3–8, 54–57].

Another aspect of great interest we are going to explore is the nature of such mechanisms. More precisely we would like to understand whether color detection

mechanisms have spectrally *broad* or *narrow* sensitivities, where the classification reflects a linear or a non-linear combination of photoreceptoral inputs. Results of physiological studies seem to agree on the fact that the majority of color-sensitive neurons combine cone signals linearly [26, 54]. However there are studies that point out the presence of cortical neurons with narrow spectral band [54, 56].

As color vision concerns human perception, in the present project we have set up a psychophysical experiment, in order to investigate the behavior of human visual system.

In our experiment, threshold measurements are performed to estimate the behavior of the visual system in color detection tasks. Threshold detection measurements operate at the limit of human ability to detect a colored signal within a chromatic noise. The goal of our threshold experiments is to express this detection limit as a function of the noise properties. Doing that, we intend to characterize the mechanisms involved in these color detection operations.

The task of the observers is to detect an equiluminant chromatic Gaussian pulse superimposed to a chromatic sectored noise masker. The stimulus (see fig. 4.1), consisting of two side-by-side square elements, one showing a noise pattern and the other one constituted by the noise pattern plus signal, is displayed in the center of a colored monitor set to neutral gray. Noise properties are varied from trial to trial to characterize the spectral sensitivity of the colored signal detection mechanism.

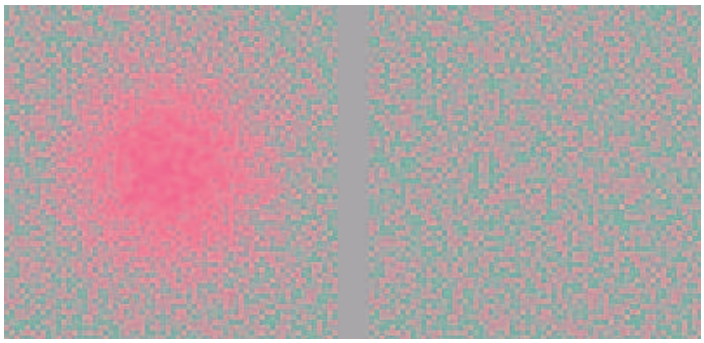

Figure 4.1: A stimulus used in the experiment.

4.3 DKL Color Space

The DKL color space was presented in sec. 2.3.4. This color space, introduced by Derrington et al. [26] in 1984, characterizes the output of the retinal processing of the human vision system, according to the opponent-color model. The axes of this color space are the three *cardinal directions*.

The axes represent approximately the differential outputs of the achromatic (ΔLum), the red-green (ΔLM) and the yellow-blue (ΔSm) mechanisms. ΔLM and ΔSm cone axes define an equiluminant plane that is centered in the reference gray point **G**. The

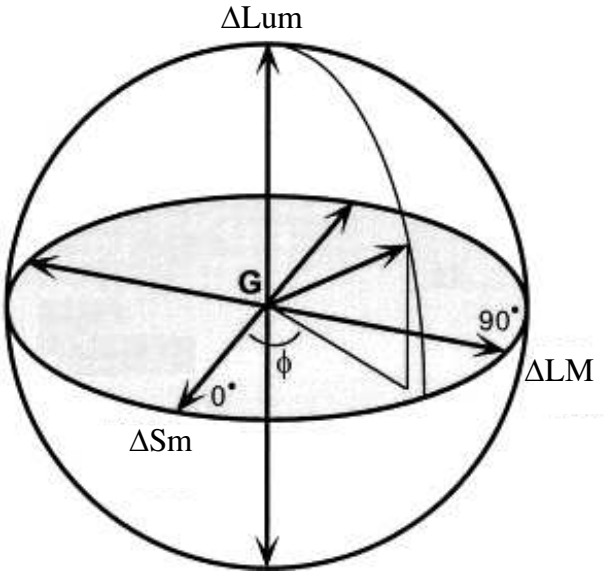

Figure 4.2: Color space of Derrington et al.(DKL).

achromatic axis is orthogonal to the equiluminant plane and intersects it at **G**. Each color in the equiluminant plane is completely defined by a vector whose modulus, ρ, is the distance between the point that represents the color and the reference gray, and whose direction, indicated by the angle ϕ, is the angle that the vector forms with the ΔLM axis. The modulus of the vector is the *contrast* of the considered color, as it represents the color saturation with respect to the reference gray **G**, while the azimuth ϕ indicates approximately the hue.

4.4 Linear Mechanisms

A mechanism that combines linearly the signals coming from the cones can be represented in the DKL color space with a vector [58]. In fact, the *response of a linear mechanism*, R, to a given stimulus can be written as:

$$R = W_{LM}S_{LM} + W_S S_S + W_{Lum}S_{Lum} \tag{4.1}$$

where W_{LM}, W_S and W_{Lum} are weights, that may be positive or negative, that the mechanism gives to the different stimulus components, and S_{LM}, S_S and S_{Lum} are the stimulus coordinates in the DKL color space. Since we investigate chromatic detection mechanisms using equiluminant stimuli, the component S_{Lum} of our stimuli will be constant and can be leave out. Thus, one can write the previous equation as:

$$R = W_{LM}S_{LM} + W_S S_S = \overrightarrow{W} \cdot \overrightarrow{x} = |\overrightarrow{W}||\overrightarrow{x}|\cos(\alpha) \tag{4.2}$$

where $\overrightarrow{W} = \{W_{LM}, W_S\}$ represents the *sensitivity* of the mechanism, $\overrightarrow{x} = \{S_{LM}, S_S\}$ is the stimulus and α is the angle between $\overrightarrow{W}$ and $\overrightarrow{x}$.

The vector of weights, $\overrightarrow{W}$, will be referred to as the *mechanism vector*. The response of a linear mechanism to any stimulus $\overrightarrow{x}$ is proportional to the projection of $\overrightarrow{x}$ onto the mechanism vector $\overrightarrow{W}$.

The set of stimuli that do not activate such a linear mechanism (e.g. for which $R = 0$) form a plane called the *null plane* of the mechanism. Modulation among any lights that lie within the null plane do not activate the mechanism. This plane is orthogonal to the mechanism vector $\overrightarrow{W}$, that gives the most efficient color direction for stimulating the mechanism. Parallel to a null plane lie what are called *response level sets*. All stimuli lying in a single such set produce responses of the same extent. The null plane and non-zero response level sets of a linear color-opponent mechanism project to lines in the equiluminant plane of the DKL color space. Fig. 4.3 shows the null plane and several response level sets for a hypothetical linear mechanism $\overrightarrow{W}$ in the equiluminant plane of the DKL color space.

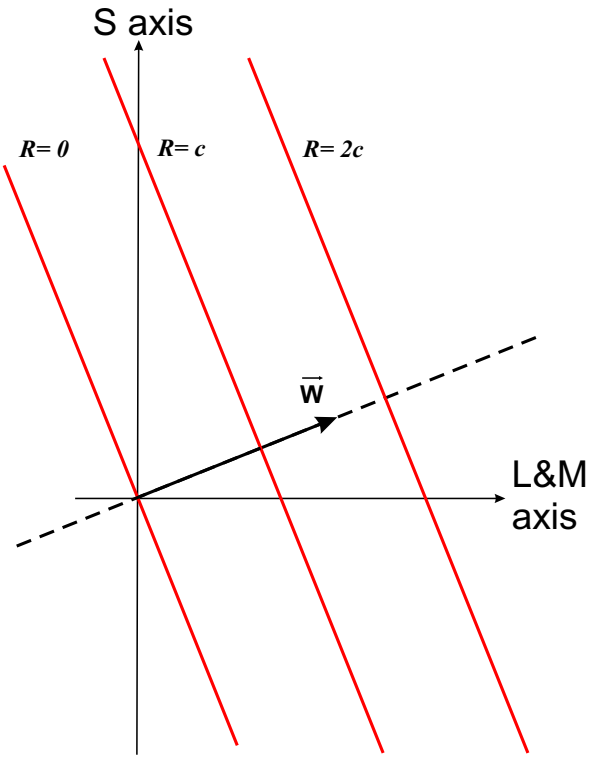

Figure 4.3: A mechanism vector $\overrightarrow{W}$ and some of its response level planes corresponding to $R = 0$, $R = c$ and $R = 2c$. The plane corresponding to a response $R = 0$ is the null plane.

A linear mechanism is also referred to as *broadband*, while a nonlinear mechanism is a *narrowband* mechanism. This is due to the fact that, from a spectral point of view, the former is sensible to a larger range of lights than the latter does. In fig. 4.4 a mechanism

vector with a linear and a nonlinear response level set are shown. The level set of the nonlinear mechanism is hypothetic, and shows just a plausible qualitative behavior of such a mechanism [3]. The hypothesized nonlinear mechanism is deduced on the basis of recent physiological studies that found cortical neurons with a similar narrowband spectral tuning [54, 56].

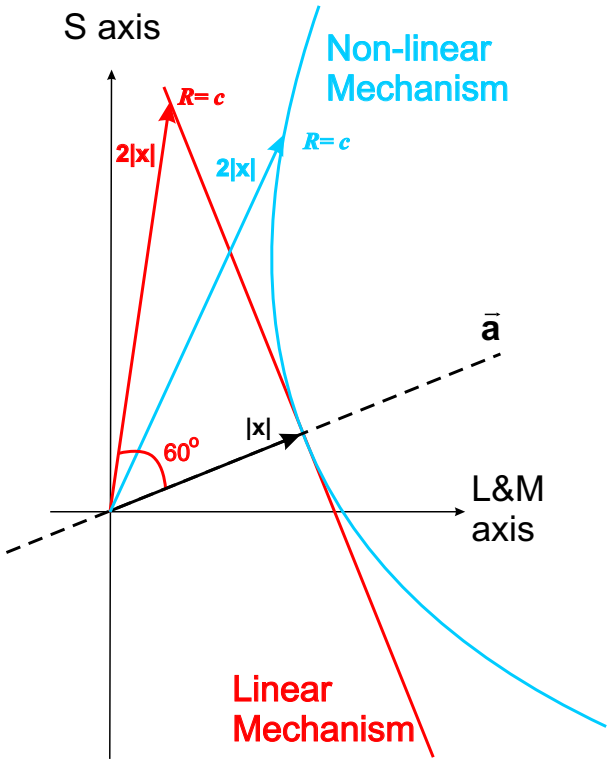

Figure 4.4: A mechanism vector in the direction $\overrightarrow{a}$ with a linear and an hypothetic nonlinear response level set.

A mechanism with its peak sensitivity in the direction $\overrightarrow{a}$ is excited to a certain level c by a stimulus of amplitude $|x|$ lying on the same direction of the mechanism vector. In the case of linear mechanism, a stimulus whose amplitude is $2|x|$ produces a response of the same extent c in the same mechanism if such stimulus is oriented 60° away from the vector of amplitude $|x|$. In the case of nonlinear mechanism, like the one represented in fig. 4.4, a stimulus of amplitude $2|x|$ induces a mechanism response of c only if the direction of the vector forms with the mechanism vector an angle smaller then 60°. This means that a linear mechanism has a chromatic broadband spectral sensitivity, while a nonlinear one possesses a narrowband spectral behavior.

One should note that, while the response of a linear mechanism to a given stimulus is influenced only by its component parallel to the mechanism vector and not by the orthogonal one, the response of a nonlinear mechanism depends on both the parallel and the orthogonal components of the stimulus light to the mechanism direction. This property

is used to characterize the chromatic detection mechanisms using a *sectored noise masking technique*, as will be explained in sec. 4.5.2.

4.5 Stimulus Creation

The stimulus consists of two side-by-side 64×64 square-element textures separated by a thin gray strip of the same chromaticity of the uniform background. One of the patches is composed of noise while the other one consists of both the signal and the noise. The properties of both signal and noise can be chosen independently of one another and change from trial to trial.

4.5.1 The Signal

The signal is a spatial isotropic Gaussian pulse with a space constant σ of 1.25° of visual angle when viewed from the fixed distance of 50 cm (see fig. 4.5).

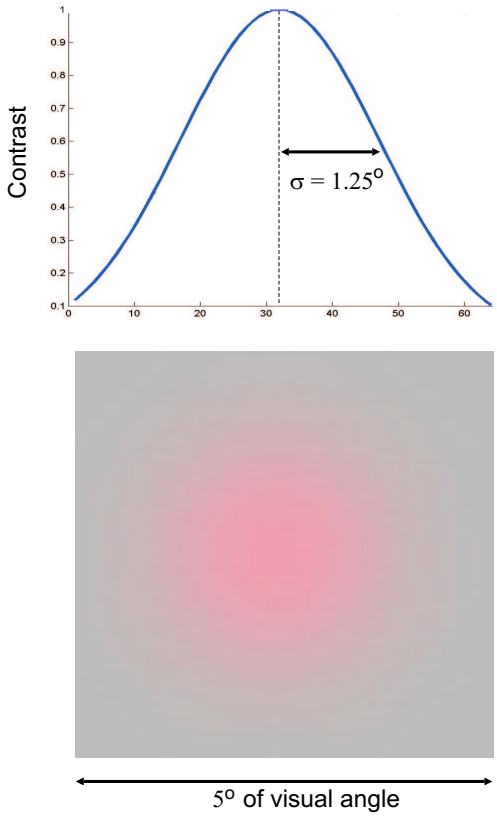

Figure 4.5: The signal and its spatial characteristics.

At the *low* spatial frequencies of the signal, the human eye is more sensitive to chromatic contrast than to black-white contrast, thus the action of chromatic detection mechanisms is emphasized, compared to that of the achromatic mechanisms.

In fig. 4.5, the azimuth of the vector representing the color in the DKL color space is 0° and corresponds to a reddish hue. The signal is 5° wide, which means that it is truncated at $\pm 2\sigma$. The Gaussian shape modulates the test color from the reference gray point to its contrast peak. The azimuth, elevation and peak contrast of the signal are under experimental control.

4.5.2 The Noise Mask

To measure the contrast thresholds for the detection of color, a *sectored noise* masking technique is used [3]. Sectored noise is generated in a way that fills a sector, centered along the chromatic direction of the tested signal, in the equiluminant plane of the DKL color space (see fig. 4.6).

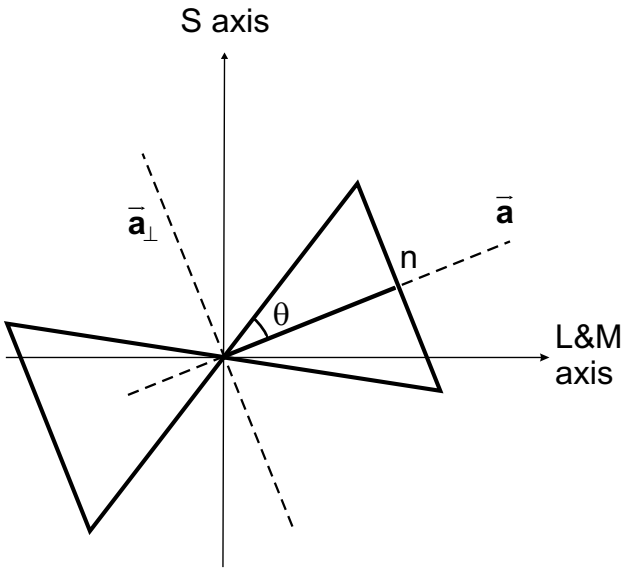

Figure 4.6: Sectored noise of amplitude n and half width θ, oriented along the direction $\overrightarrow{a}$.

To generate a sectored noise of half width θ and amplitude n, we use two random processes drawing samples from a uniform distribution on the interval $[-1, 1]$. The first one, *R(x,y)*, provides the noise component along the direction $\overrightarrow{a}$, which is the axis along which the signal is oriented. The second one, $R_\perp(x, y)$, generates the samples that provide the noise along the axis perpendicular to the signal. Thus one can describe a sectored noise $\overrightarrow{N}(x, y)$ of half width θ and noise contrast n as:

$$\overrightarrow{N}(x, y) = nR(x, y)\overrightarrow{a} + nR_\perp(x, y)\tan(\theta)\overrightarrow{a}_\perp \tag{4.3}$$

where $\overrightarrow{a}$ and $\overrightarrow{a}_\perp$ are the unit-length vectors along the chromatic axis of the signal and along the perpendicular axis.

For each element of the spatial noise pattern, the characteristics of the noise such contrast, sector width and orientation are fixed, while two random samples are generated by *R(x,y)* and $R_\perp(x, y)$ to define the chromaticity of the element itself.

When the half width of the sector, θ, is equal to zero, the sectored noise can be considered an *axial noise*. This noise provides random samples from an ensemble described by a uniform density function on the interval $[-n, n]$. The samples are used to modulate the chromaticity along the same direction $\overrightarrow{a}$ along which the signal lies. Thus, an axial noise $\overrightarrow{A}(x, y)$ of amplitude n in the direction $\overrightarrow{a}$ can be expressed as:

$$\overrightarrow{A}(x, y) = nR(x, y)\overrightarrow{a} \tag{4.4}$$

A linear mechanism tuned to the central direction $\overrightarrow{a}$ is not influenced by the $\overrightarrow{a}_\perp$ component of the sectored noise. In other words, it can not distinguish between an axial noise and a sectored noise of the same amplitude n. This can be shown by computing the dot product of a mechanism vector, say $\overrightarrow{W} = m\overrightarrow{a}$, and the right-hand side of eq. 4.3:

$$\begin{aligned} \overrightarrow{N}(x, y) \cdot \overrightarrow{W} &= \{nR(x, y)\overrightarrow{a} + nR_\perp(x, y)\tan(\theta)\overrightarrow{a}_\perp\} \cdot \{m\overrightarrow{a}\} \\ &= nmR(x, y) \end{aligned} \tag{4.5}$$

The noise modulation along the perpendicular axis $a_\perp$ produces zero response.

By holding constant the noise modulation along the central axis $\overrightarrow{a}$ and varying the width of the sector θ, one can test whether there are departures from such linearity. In fact, the performances of a linear mechanism should not be affected by variations of the sector half width θ. On the other hand, a nonlinear mechanism should be influenced by sector width variations. More particularly, if the nonlinear mechanism has the hypothesized behavior shown in fig. 4.4, one can see that an increase in sector half width θ should lead to a decrease in noise masking efficiency. Fig. 4.7 illustrates graphically this phenomenon.

Any color inside the sector, for example the one determined by the vector $\overrightarrow{s}$, produces in the mechanism tuned to the direction $\overrightarrow{a}$ a response, for example b, which is smaller or equal than a, which is the mechanism response produced by an axial noise (i.e. $\theta = 0$) of the same amplitude of that of the sectored noise.

Note that such a technique allows not only to estimate if a chromatic mechanism is linear or not, but also to understand if the detection of color signals with *non-cardinal chromaticities*, like orange, is mediated by *intermediate* higher order mechanisms as opposed to by two classical cardinal mechanisms. In fact, testing an intermediate direction $\overrightarrow{a}$ of the color space, one can observe that an increase in sector half width θ should lead to an increase in noise masking efficiency. When the sector width increases, the projections of noise components on the two mechanisms mediating color detection become bigger. In fig. 4.8, a graphical example is diagrammed.

In this example, the maximum noise contrast levels perceived by the red-green and the yellow-blue mechanisms in case of axial noise (i.e. $\theta = 0$) are m and n respectively.

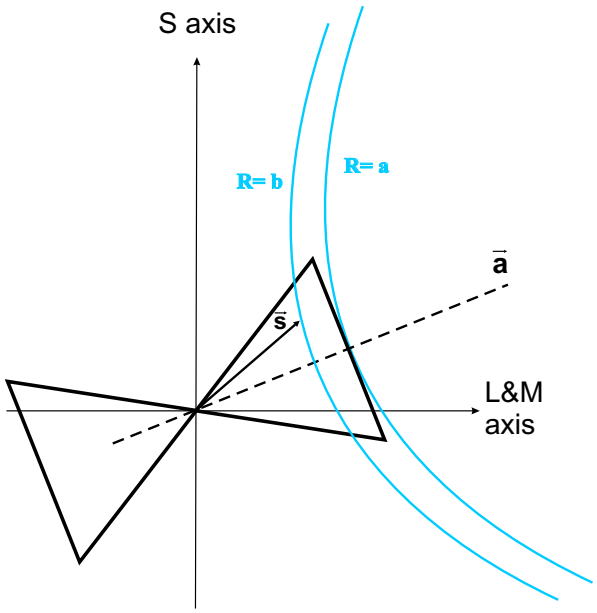

Figure 4.7: Two hypothetical level sets of a nonlinear mechanism. When the noise sector width increases, the masking efficiency decreases. Any color inside the sector produces in the mechanism tuned to the direction $\overrightarrow{a}$ a response $b \leq a$, where a is the mechanism response produced by an axial noise ($\theta = 0$) as strong as the sectored noise.

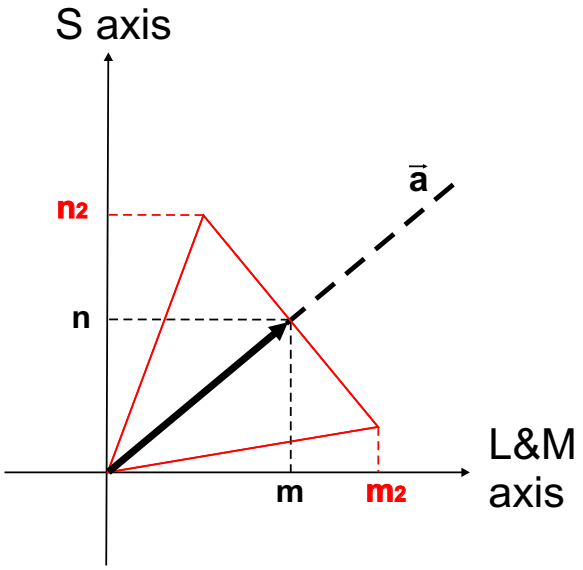

Figure 4.8: Sectored noise masking with only two cardinal mechanisms. Increasing the sector width, noise masking efficiency should increase.

Increasing the sector half width θ, the maximum noise levels perceived by the two mechanisms raise up to m_2 and n_2 respectively. Thus, an increased masking effect is expected, increasing sector half width θ.

In summary, one can distinguish between three cases:

1. A **linear** mechanism tuned to the considered direction $\overrightarrow{a}$ mediates the detection. Thus, noise masking efficacy is independent on the noise sector half width θ.

2. A **nonlinear** mechanism whose sensitivity lies along the considered direction $\overrightarrow{a}$ is responsible for the detection. Thus, noise masking potency declines, increasing the noise sector half width θ.

3. Chromatic detection is mediated by **two cardinal** mechanisms. Thus, with the increase of the sector half width θ, the sensitivity to noise masking rises.

4.5.3 The Stimulus

When a signal $\overrightarrow{S}(x,y)$ of contrast s along the direction $\overrightarrow{a}$ is added to the sectored noise, we obtain a spatial pattern $\overrightarrow{W}(x,y)$:

$$\begin{aligned} \overrightarrow{W}(x,y) &= \overrightarrow{S}(x,y) + \overrightarrow{N}(x,y) \\ &= s\overrightarrow{a} + nR(x,y)\overrightarrow{a} + nR_{\perp}(x,y)\tan(\theta)\overrightarrow{a}_{\perp} \\ &= \{s + nR(x,y)\}\overrightarrow{a} + nR_{\perp}(x,y)\tan(\theta)\overrightarrow{a}_{\perp} \end{aligned} \tag{4.6}$$

In fig. 4.9 the stimulus, consisting of a noise pattern (on the left) and of a signal plus noise pattern (on the right) is shown. In the upper part of the figure, the chromatic coordinates of all the elements of the stimulus are diagrammed.

The stimulus is approximately 10.5° of visual angle. At the viewing distance, the resolution is approximately 2' per pixel and each square element (3×3 pixels) subtends 6' of visual angle. Thus, the spatial frequency of the stimulus is approximately 5 cycles/degree: at these frequencies, the human eye can clearly distinguish the chromaticities of the different elements. The stimulus is displayed on a uniform gray background whose coordinates in the DKL color space are those of the reference gray point in the equiluminant plane. The central strip, 0.5° wide, separates the two patterns that form the stimulus and has the same chromaticity of the background. A fixation point is displayed in the center of the image in order to ensure that the same region of the fovea is involved in every detection task.

4.6 Apparatus

Stimuli are created with Matlab 6.1 on a Windows computer. The experiment is controlled using WinVis for Matlab, a psychophysical testing platform developed by the Neurometrics

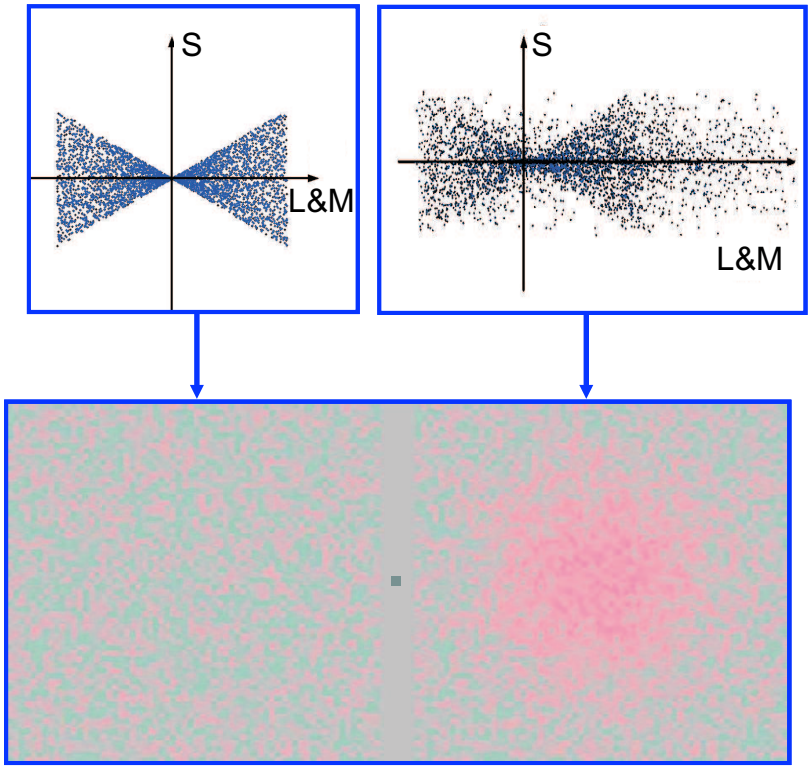

Figure 4.9: A stimulus obtained with signal azimuth $\phi = 0°$ and noise sector half width $\theta = 30°$. The chromaticities of the noise pattern (on the left) and of the signal plus noise pattern (on the right) are also diagrammed.

Institute (Berkeley, CA, USA). This tool can combine stimuli into elaborate trials and experiments. With WinVis, one has specific control over display settings such as resolution and bit depth, and can precisely control the timing of the experiment.

The screen is a Barco PCD 321 Plus 21" monitor. The coordinates of the three phosphors, measured in CIE 1964 XYZ, are given in table 4.1. In fig. 4.10, the maximum values of the three phosphors and of the reference grey are plotted in a *xy* diagram. The *gamut* of the monitor, consisting of all the possible displayable combinations of the phosphors values is also plotted.

Images are displayed on the monitor by a standard video board with 8-bit digital-to-analog converter. The screen was set on 1024 high $\times$ 1280 wide pixels video mode.

	x_{CIE31}	y_{CIE64}	Max. Luminance in cd/m^2
RED	0.6182	0.3425	20.3562
GREEN	0.3179	0.5932	51.5282
BLUE	0.1452	0.0905	9.8561

Table 4.1: Color coordinates of monitor phosphors in CIE 1964 XYZ.

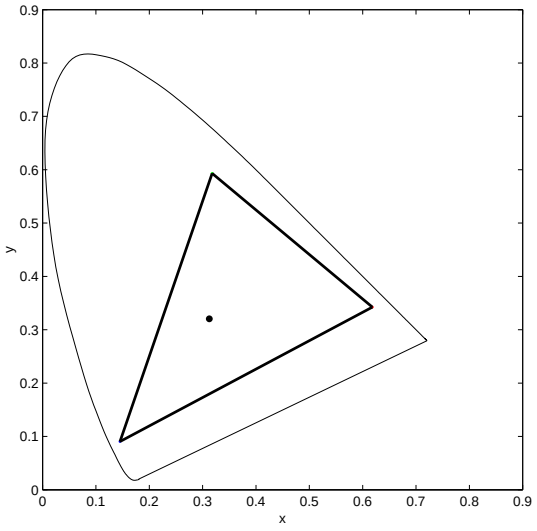

Figure 4.10: The gamut of the monitor plotted in a *xy* diagram.

4.6.1 Calibration and Characterization

The characteristics of the phosphors were measured with a Minolta CS-1000 spectroradiometer. That apparatus can measure spectral responses each nanometer in the range between 380 nm and 780 nm with a precision of 0.3 nm. The calibration measures have been done on 17 patches for each color: red, green, blue and gray. The 17 chromaticities of the patches comes from a uniform quantization of the whole dynamics of the screen. In fact, to characterize the monitor we used a C code developed in the laboratory. This program allows an automatic synchronization between the displaying of the stimulus on the screen and the measure of the Minolta spectroradiometer. The measured spectra are shown in fig. 4.11.

The spectral information is essential to have data for the color coordinate transformation and to *gamma(γ)-correct* the screen nonlinearity. In fact, in order to control as much as possible the performances of our system, we perform a specific transformation from the RGB values of our monitor to the DKL color space, where the stimuli are defined.

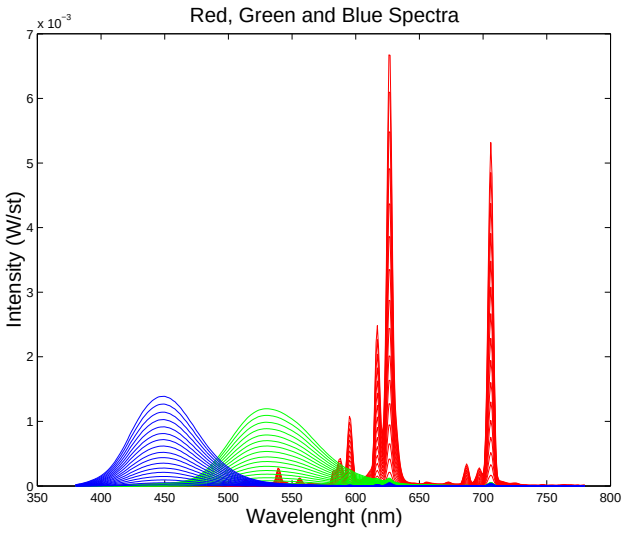

Figure 4.11: Measured spectra for the Barco PCD 321 Plus display. The measures have been effectuated with a Minolta CS-1000 spectroradiometer.

Gamma-correction

The nonlinear relationship between the applied voltage and phosphor intensities is $\gamma -$ *corrected* evaluating the gamma function for each gun of the Barco display. In fact, a *cathode-ray tube* (CRT) is inherently nonlinear: the intensity of the light reproduced at a CRT screen is a nonlinear function of its voltage input. Instead, the intensity produced by a CRT is proportional to the input voltage raised to the power γ, following the relation:

$$\mathbf{Y} = (a + b\mathbf{S})^{\gamma} \tag{4.7}$$

where $\mathbf{Y}$ is the measured luminance, $\mathbf{S}$ is the digital value, that can take values from 0 to 255, and a, b and γ are the parameters to be estimated. Thus, the gamma-correction can be thought of as a compensation for this nonlinearity, in order to achieve a correct, linearized reproduction of color intensity.

From Linearized RGB to LMS

Once we have linearized values of RGB, it is possible to find an *ad hoc* transformation matrix that transforms points defined in the DKL color space into linear RGB stimulations for our monitor.

The Moore-Penrose [59] procedure is used to find the transformation matrix that best maps the stimulus in RGB coordinates to XYZ coordinates, minimizing the least square error. The XYZ data we use are represented in the CIE 1964 10° color space, as the stimulus is about 10° wide. Thus, the transformation 3×3 matrix T can be found as:

$$T = (RGB^{\top} \cdot RGB)^{-1} \cdot RGB^{\top} \cdot XYZ \tag{4.8}$$

where RGB and XYZ are $n \times 3$ matrices representing n different colors expressed in RGB coordinates and in XYZ CIE 1964 coordinates.

Another transformation matrix from XYZ CIE 1964 coordinates to LMS coordinates is calculated using the cone fundamentals measured by Stockman et al. in 1993 [60].

Both these transformations are applied to relate the RGB coordinates of the monitor with the LMS color space and then to the DKL color space which is a simple linear combination of the LMS color space.

The details of the procedure are shown in Appendix A.

4.7 Observers

The threshold measurements were made by six color-normal observers. Normal color discrimination was assessed with the Farnsworth-Munsell 100 Hue Test, described by Farnsworth in 1943 [61]. The are 85 *chips* or color samples, divided into four sets; these 85 chips represent just-noticeably-different steps for subjects with normal color vision. The subject is told to arrange the caps between two fixed end caps in order of color appearance. A score is computed, that gives an idea of the chromatic vision of the subject. If this score is very low, it means that the observer has done very few errors and he is classified *superior discriminator*. If the score is average, the observer is classified *average discriminator*, while if the score is quite high, the observer has chromatic discrimination problems and cannot be considered for our detection experiments.

There were two male observers (IO and NP) and four female observers (ES, GM, PG, ED). Three of them (IO, GM and PG) were familiar with psychophysical experiments, while the others were naïve.

4.8 The Procedure

To make a psychophysical test, a very strict protocol should be followed, in order to control as much as possible the variables involved in the experiment. A large number of elements can influence the observer's judgement, like his/her reliability, the viewing conditions, or even the comfort of the location.

Observers were sitting in a completely dark room at 50 cm from the screen. The experiments were done in absence of light to assure a constant illumination for all the tests and all the subjects. The fixed viewing distance is required to control the spatial frequency of the stimulus and to ensure uniform viewing conditions, in order to reduce any source of variability.

The screen was set to a uniform gray background on which the instructions for the experiment, which had been previously explained, were displayed. Subjects were asked to judge on which side of the fixation point the signal, a Gaussian blob, was displayed, in a

stimulus like the one shown in fig. 4.1. On one side of the stimulus, the signal added with a chromatic sectored noise is presented, while only the noise is displayed on the other one. A task like that is called two alternative forced choice task. The observers were asked to fix the central reference point, in order to ensure that the region in the subjects' fovea involved in the detection task is always the same and thus control this other possible cause of variability. After 30 sec a short trial test was started, to get the subject familiar with the protocol of the experiment and adapted to the gray background.

At this point, the "real" experiment started. Observers viewed a stimulus and were asked to answer on which side of the stimulus they believed the Gaussian pulse signal to be present. After answering, the stimulus disappeared, the gray background was displayed for some seconds and a new stimulus was shown. This procedure was adopted because it was observed, during some pilot tests, that the subjects had the tendency not to detect the signal itself but its *afterimage* (see sec. 3.2.2) when the stimulus disappeared. The fact of not providing a fixed viewing time for each stimulus could be a source of variability between subjects and between different experiments; for that reason, subjects were asked to answer as soon as they could detect the signal. For each trial, noise amplitude n, signal azimuth ϕ and noise sector half-width, θ, are held constant. The signal contrast, ρ, is varied from stimulus to stimulus within each trial following an adaptive staircase (see fig. 4.12) and is initialized to an arbitrary value. For the first three stimuli the increasing/decreasing step is half of the signal level; one correct answer leads to a reduction in the signal contrast while one incorrect answer leads to an increase in the signal contrast on the following trial. After the third presentation, the "rule" is changed: the step becomes the 20% of the signal level and a reduction in signal contrast follows three correct answers in a row. A wrong answer still leads to a signal contrast increase. Such a method allows to quickly reach the threshold region.

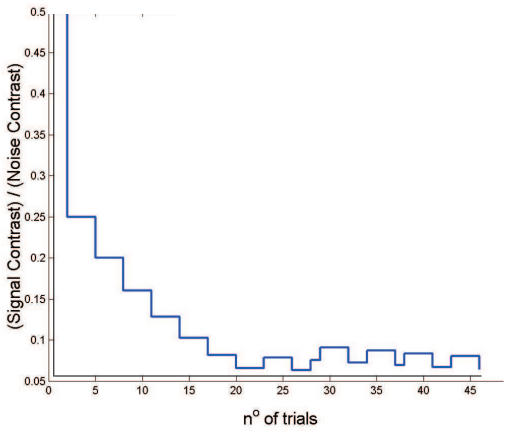

Figure 4.12: A typical staircase. The signal contrast is normalized to the given noise contrast. After some stimuli, the staircase oscillates around the threshold value.

Each staircase (or trial) is made of 48 stimuli; in a staircase, threshold is estimated for a particular combination of the experiment parameters n, ϕ and θ. The trials were run interleaving the color directions.

The values chosen for the color azimuth ϕ are 0° and 90°, which are two of the cardinal directions individuated by Krauskopf et al. [4] and two intermediate directions. One of these directions was estimated by some pilot tests; this was the one at which the two mechanisms along the cardinal directions were estimated to have equal sensitivity for observers IO and GM. This direction was estimated from the contrast thresholds without noise in each cardinal direction (red and yellow), calculating the intersection of the perpendicular lines going through the threshold on each axis. Such intermediate color direction was defined by a color angle ϕ of 15°. The other chromatic direction has been chosen as it was the direction which described a color that perceptually looks orange. This was characterized by a ϕ of 75°. For each color direction, 4 levels of noise (n) were considered, from zero to the maximum value displayable by the monitor in each color direction ϕ. The values that the monitor can represent are all those lying inside the contour plotted in fig. 4.13, that is called the *gamut* of the monitor. Thus, the color values inside the DKL gamut produce RGB linearized (and normalized) monitor values that are *real*, positive and smaller than one.

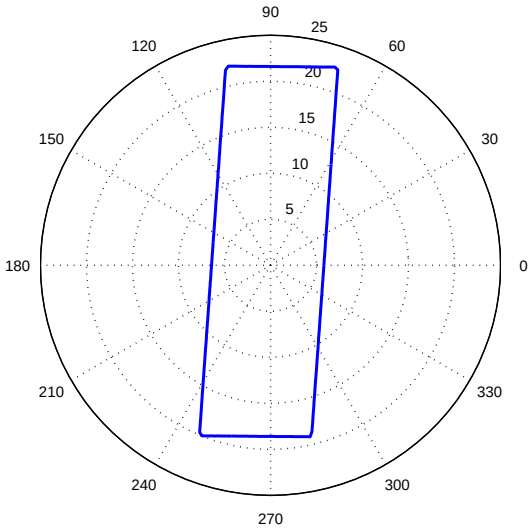

Figure 4.13: The monitor gamut in the DKL color space.

The intermediate values of n were empirically chosen with some pilot run to have a sufficient noise level to raise the threshold. These were 1/2 of the maximum noise level available and 3/4 of the maximum. The noise half-width angle θ took the values 0^o, 30^o and 60^o.

Each subject tested all the conditions, thus a complete series was made of 40 staircases, 10 for each color direction tested. Subjects ED and NP performed reduced series of 30 staircases as they tested just three color directions instead of four. For each color, the

no-noise condition was tested and all the combinations of the three noise levels n with the three noise sector widths θ. Subjects took pauses about every 12 minutes not to get tired or stressed. Each observer effected four series, except for one (NP), that completed only three series. The first series was not considered in the statistics because resulted very noisy. This is probably due to the difficulty of the task: observers had to get familiar with the experiment and experience their detection mechanisms.

All the conditions tested in the psychophysical experiment are summarized in table 4.2.

Number of subjects	Color directions ϕ tested by each subject* (Azimuth in deg.)	Sector widths θ tested for each color direction (in deg.)	Noise levels n tested for each combination of ϕ and θ (referred to $max^{\dagger}$)
6	0°, 15°, 75°, 90°	0°, 30°, 60°	0, 1/2 max, 3/4 max, max

Table 4.2: All the values taken by the parameters in the experiment. *Observers ED and NP tested three color directions ϕ (ED did not test $\phi = 75$, NP did not test $\phi = 15$). $^{\dagger}max$ is the maximum value displayable by the monitor in each direction ϕ.

4.9 Conclusions

This chapter detailed how the psychophysical experiment has been set up. We have re-introduced the DKL color space, where the stimuli used for the tests were designed. A review of the liner mechanisms in the DKL color space has been done, and also a description of nonlinear mechanisms.

A detailed description of how the signal and the noise mask were generated has been furnished, with particular attention to the sectored noise masking technique that has been employed for these threshold measurement tests. Then, in the last sections we have described carefully the protocol of the psychophysical experiment and the apparatus has been described and characterized.

Chapter 5

Analysis and Results

5.1 Introduction

In this chapter we present and analyze the results of the psychophysical tests that have been carried out.

In the previous chapter we have introduced the procedures used to set the experiment, build the stimuli and carry out the tests. In the present one, the results of the psychophysical experiments are shown, analyzed and discussed. In section 2 we show how the data from the experiments have been collected and represented. To interpret the data, we have fitted it to a noise masking regular model proposed by Pelli [62] and Legge et al. [63]. We have therefore compared the results of the fits made under two different hypotheses on the mechanisms mediating color detection, using a special *likelihood ratio test*. The third section presents the noise masking model used to fit the data, the results of the fitting and the evaluation of such a fitting through a *nested fitting technique*.

5.2 Threshold Measurement

Using the two alternative forced choice (2AFC) procedure described in chapter 4, thresholds for chromatic signal detection have been measured.

Once the parameters of the experiment, test color azimuth ϕ, noise contrast n and sector half width θ, have been fixed, one can estimate the signal contrast at threshold in those specific conditions for each observer. This has been done for every possible combination of the parameters, holding to 40 thresholds estimated, one for each condition, for each complete series of experiments.

Fig. 5.1 shows a typical staircase profile; the signal contrast levels used in one experiment, normalized to the given noise contrast value, are plotted as a function of the trial number.

It can be noted that, after a *transient*, the signal values start to oscillate around a certain value, called t. The oscillation is due to the fact that the observer can detect the signal within the noise mask when the signal contrast is greater than such value, while

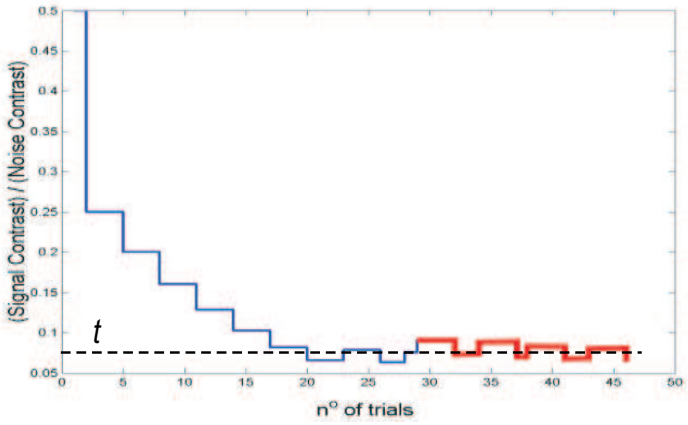

Figure 5.1: A typical staircase; the signal contrast is normalized to the given noise contrast. The values in red are those used to estimate the threshold for that particular staircase.

he can not when the signal contrast is smaller. Thus, this value t is expected to be the *threshold* for the observer in these particular conditions.

We have estimated the thresholds averaging the staircase values after a certain *stabilization*. We arbitrarily considered the staircase stabilized when it has effected three *reversals*, which means, when the subject gave three wrong answers (see fig. 5.1).

Each subject performed four complete series of 40 staircases, except for one observer that performed three. As discussed in sec. 4.7, the first series is not considered in the statistics because it is very noisy. This was an unexpected phenomenon, probably due to the difficulty of the detection experiment. In fact, observers had to get familiar with such a hard task and experience their chromatic detection capabilities. In fig. 5.2 signal contrasts at threshold for observer IO are plotted as functions of noise contrast. Signal color azimuth ϕ and noise sector half width θ were fixed and took the values respectively of 0° and 30°. Results for the four different series are diagrammed with different colors. The data are plotted in a classical log-log scale, typically used for this kind of graphics [3–5].

To obtain one threshold value for each observer in each specific condition, a mean threshold value μ is calculated. This average value has been computed from three thresholds measured in the last three series of experiments. Thus, for every testing condition, one has a set of points like the one in fig. 5.3 (a). Each data point μ has its own standard deviation σ, which is calculated as:

$$\sigma = \sqrt{\frac{\sum_{i=1}^{N}(v_i - \mu)^2}{N-1}} \tag{5.1}$$

where N is the number of values considered to compute the mean threshold μ (in our case, 3) and v_i are the threshold values measured in a single series.

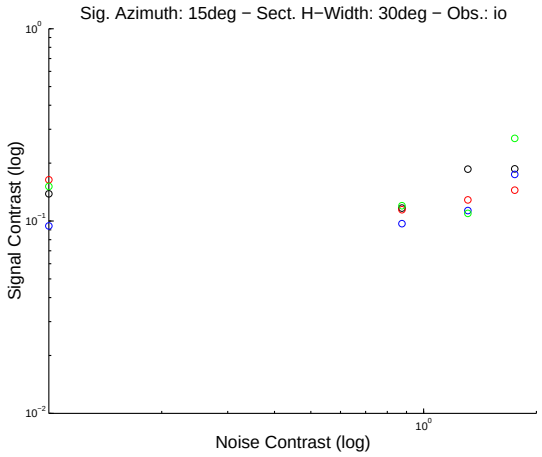

Figure 5.2: Signal contrasts at threshold plotted as a function of noise contrast in a log-log scale. The observer, the signal color azimuth ϕ and the noise sector half width θ are fixed. The results for four different series are diagrammed with different colors.

We have used a sectored noise masking technique to estimate whether chromatic detection mechanisms tuned to intermediate directions of the color space exist and to understand if such mechanisms combine cone signals in a linear fashion or not. We have observed (see sec. 4.5.2) that, if the performances of human visual system in color detection tasks are not influenced by the width of noise sector, then the color mechanism mediating such a detection should be tuned to the signal direction and should combine the cone outputs linearly. Thus, in order to compare the results for different values of noise sector half width θ, the data have been plotted in diagrams like the one in fig. 5.3 (b).

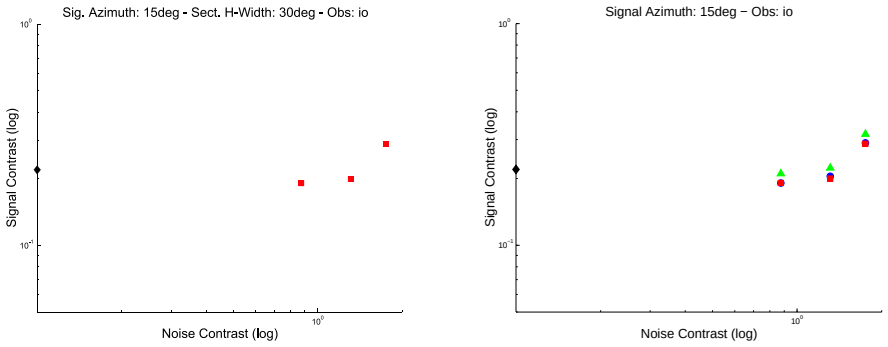

(a) (b)

Figure 5.3: Signal contrasts at threshold (mean) plotted as a function of noise contrast in a log-log scale. In figure (a), data points for subject IO with $\phi = 15°$ and $\theta = 30°$ are plotted. Figure (b) shows data points for observer IO at $\phi = 15°$ for $\theta = 0°$ (blue circles), $\theta = 30°$ (red squares) and $\theta = 60°$ (green triangles) drawn together.

In those plots, we have drawn all the data points for one observer for one color direction ϕ. Blue circles correspond to threshold levels with $\theta = 0°$, red squares indicate the $\theta = 30°$ condition, and green triangles the $\theta = 60°$ condition.

5.3 Results

There have been several studies in which contrast thresholds were measured in the presence of visual noise masking. In such experiments [3, 62, 63] it has been shown that the relationship between signal detection threshold s and noise contrast n is represented well by the equation:

$$s^2 = e_0 + kn^2 \tag{5.2}$$

where the slope k and the intercept e_0 are parameters estimated from the data. Thus, detection thresholds result not to be influenced by noise masking at low noise levels. Then, thresholds rise following a linear relationship between the squares of signal and noise contrasts, as expressed by eq. 5.2 and depicted in fig. 5.4.

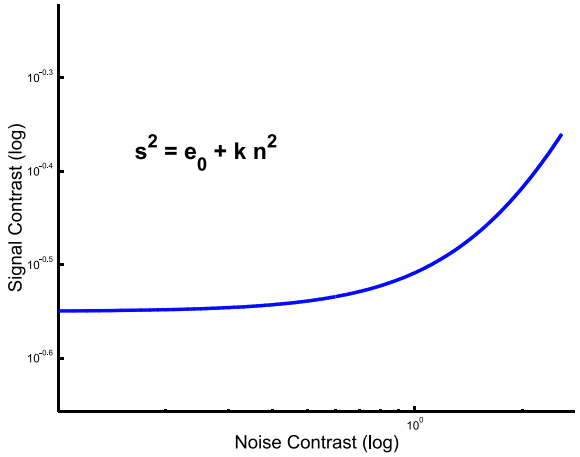

Figure 5.4: Typical representation of signal contrast at threshold as a function of noise contrast in a log-log space.

The noise level at which thresholds start to increase has been interpreted by Pelli [62] and Legge et al. [63] as the intrinsic noise of the detection mechanism. This noise may be associated with the transduction from visual stimulus to neural signal or could be related to the decision process itself [63].

This regular relationship between signal contrast at threshold and noise contrast is used to describe the data from our experiments. Thresholds have been estimated for four colors (two nuances of red, orange and yellow) increasing sectored noise levels and varying noise sector width. Eq. 5.2 describes well the data measured in the psychophysical tests.

We fitted those data with the relationship expressed by 5.2 to determine the behavior of chromatic mechanism in the presence of the noise mask for different values of sector half width θ. In fact, we wanted to understand whether noise masking efficacy depends on sector width or not. The independence of masking efficacy from sector width is a feature of linear, broadband chromatic mechanisms, while the loss of such effectiveness indicates that color detection is mediated by a narrowband, thus nonlinear, mechanism. Finally, when testing an *intermediate* color direction, i.e. orange, an increase in noise masking efficacy with increasing noise sector width indicates that detection must be mediated by two linear cardinal mechanisms.

5.3.1 The Reddish Signal (azimuth of 15°)

One color tested is the *reddish* signal with azimuth $\phi = 15°$ in the equiluminant plane of the DKL color space. The measured thresholds for four observers (IO, ES, GM and PG) for the color direction $\phi = 15°$ are diagrammed in fig. 5.5.

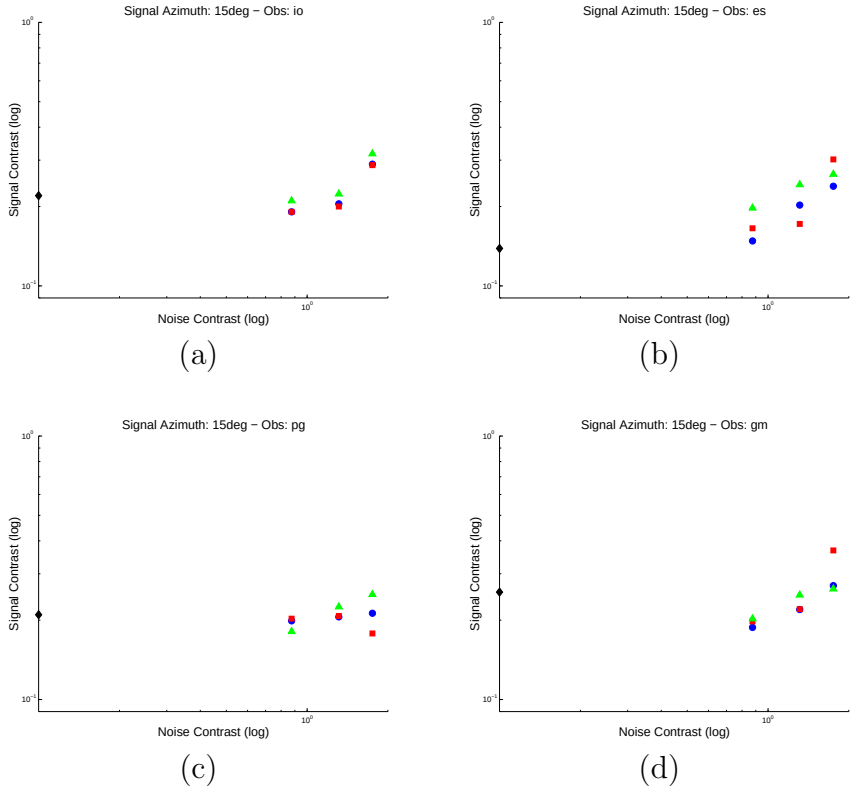

Figure 5.5: Signal contrasts at threshold plotted as functions of noise contrast for an azimuth $\phi = 15°$, in a log-log scale. Noise masking functions were estimated for sector half width $\theta = 0°$ (blue circles), $\theta = 30°$ (red squares) and $\theta = 60°$ (green triangles). In fig. (a), data point for subject IO are plotted. Fig. (b) shows data point for observer ES, fig. (c) those of observer PG and fig. (4) results for observer GM.

This color direction has been determined to be the one along which the two cardinal mechanisms are estimated to have equal sensitivity (see sec. 4.7). When viewed in isolation, such signal appears light red.

Noise masking functions were estimated for each of the observers for sector half width $\theta = 0°$, $\theta = 30°$ and $\theta = 60°$. The data points for different sector widths θ are plotted with different shapes and colors. Those results are the means of thresholds determined by three staircases.

The results shown in fig. 5.5 suggest that masking efficacy does not depend on sector width; data points at the same noise contrast level for different sector widths θ are close one to the other. Besides, no systematic trend comes out from the position of the markers representing the data for different θ. To quantify how noise sector width influences noise masking efficacy, the model expressed by eq. 5.2 was fitted to the data points for each half width θ. Two different models were therefore fitted to the data using a least-squares fitting. Finally, these two models were compared using a *nested fitting technique*.

5.3.2 Fitting the Data

Here we want to test how *good* is the hypothesis that the performances of chromatic mechanisms in detecting a colored signal masked by sectored noise are not influenced by the width of such sector. Thus, we have first fitted the model of eq. 5.2 with the data for each sector width *independently*: this is what we have called *local fitting*. We have not assumed that the noise masking efficacy is independent of sector width and we fitted the model with three sets of data, one for each sector half width θ. Fig. 5.6 shows the results of such a fit procedure for observers IO and ES.

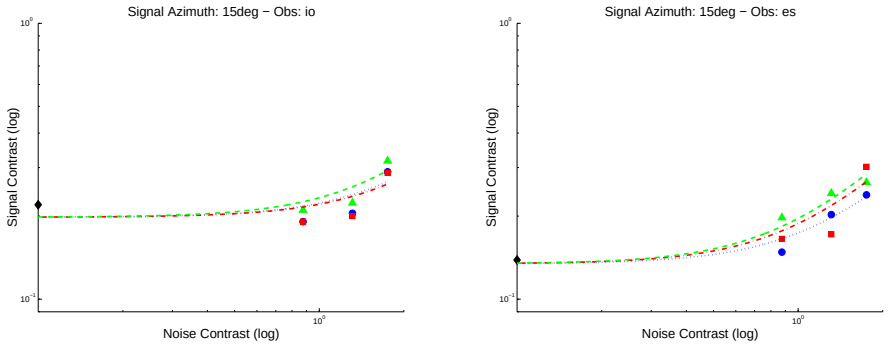

(a) (b)

Figure 5.6: Signal contrasts at threshold plotted as functions of noise contrast in a log-log scale. "Local"" fitting curves were estimated for sector half widths $\theta = 0°$ (blue dotted line), $\theta = 30°$ (red dash-dotted line) and $\theta = 60°$ (green dashed line). In fig. (a), fitting curves for subject IO are plotted. Fig. (b) shows the fitting curves for observer ES.

The fitting was done minimizing, in the least square sense, the χ^2 value computed between the measured thresholds and the expected values from the model of eq. 5.2. Thus, the χ^2 quantity was computed as:

$$\chi^2 = \sum_{i=1}^{N} \left(\frac{s_i - f(n)}{\sigma_i} \right)^2 \tag{5.3}$$

where N is the number of considered points, s_i are the measured thresholds, $f(n)$ are the expected threshold values, for the correspondent noise level n, following the model, and σ_i are the standard deviations of the the measured data points. Thus, substituting $f(n)$ in eq. 5.3 with the expected contrast value from eq. 5.2, the quantity to minimize was:

$$\chi^2 = \sum_{i=1}^{N} \left(\frac{s_i - \sqrt{e_0 + k_\theta n^2}}{\sigma_i} \right)^2 \tag{5.4}$$

where e_0 and k_θ are the parameters to estimate. To fit the model with the data *independently* for each sector width means that we have to estimate four parameters: the intercept e_0 and three slopes k_θ, one for each sector half width θ. We have computed one intercept for all the data because this point indicates the square of the signal contrast at threshold in the no-noise condition ($n = 0$), and it seems logical to assume that it is the same for all the sector widths. On the other hand, if one assumes that the color detection mechanism behavior depends on the width of the sectored noise, three different slopes have to be estimated.

The χ^2 value for the local fitting has been calculated following the expression of eq. 5.3. We call this value χ^2_{LOC}. Then, to have a *quantitative* measure of agreement between the observed data and their expected values, we have calculated the *probability* of obtaining a value of χ^2 as large as, or larger than, our value χ^2_{LOC} [64]. This probability depends on the number of *degrees of freedom* of the experiment. In general, the number of degrees of freedom d in a statistical calculation is defined as the number of observed data minus the number of parameters estimated from the data and used in the calculation. Here we have ten data points and four parameters, thus $d = 10 - 4 = 6$. Assuming that the observed data are distributed around their expected values according to a *Gaussian distribution*, one can compute the probability that a χ^2 value calculated for an experiment with d degrees of freedom is greater or equal than χ^2_{LOC} as [64]:

$$P_d(\chi^2 \geq \chi^2_{LOC}) = \frac{2}{2^{d/2}\Gamma(d/2)} \int_{\chi^2_{loc}}^{\infty} t^{d-1} e^{-t^2/2} dt \tag{5.5}$$

where $\Gamma(z)$ is the generalization of the *factorial function* to real and complex arguments:

$$\Gamma(z) = \int_0^{\infty} t^{z-1} e^{-z} dt \tag{5.6}$$

There is no closed form solution for $P_d(\chi^2 \geq \chi^2_{LOC})$, so it must be evaluated numerically.

Thus, if the computed probability $P_d(\chi^2 \geq \chi^2_{LOC})$ is large, there is no reason to reject the assumed model: if it small, there is an high probability that the model does not represent carefully the data. In particular, if $P_d(\chi^2 \geq \chi^2_{LOC})$ is less than 5 percent, we say the disagreement is *significant*, and the assumed model is rejected *at the 5 percent level*. For all our experiments, we have found values of $P_d(\chi^2 \geq \chi^2_{LOC})$ greater than 95 percent, thus the *local model* cannot be rejected, it fits well the data.

As a second step, we have estimated the fit for all the data points together, assuming that the variation of the sector half width θ does not influence the mechanism performances. This behavior is consistent with the existence of linear broadband mechanisms mediating chromatic contrast detection. Under this hypothesis, only one value of the parameter k for all the data has to be estimated and thus, only one fitting curve is computed: this is what we have called *global fitting*. The *global fitting* curves for the data of fig. 5.6 are plotted in fig. 5.7.

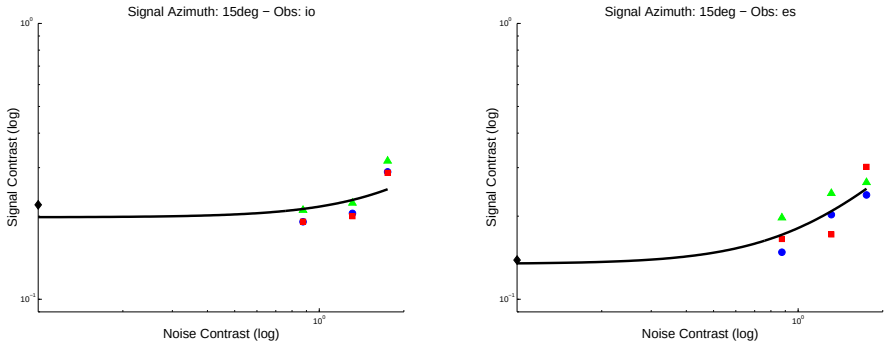

(a) (b)

Figure 5.7: Signal contrasts at threshold plotted as functions of noise contrast in a log-log scale. The "global" fitting curves are plotted for subjects IO (a) and ES (b).

The same statistics than in the local fitting case have been computed. Thus, we have calculated the χ^2 value for that fitting, let us call it χ^2_{GLOB}, and the probability $P_d(\chi^2 \geq \chi^2_{GLOB})$ with $d = 10 - 2 = 8$ degrees of freedom, as only two parameters have been estimated in this case. Again, the values of $P_d(\chi^2 \geq \chi^2_{GLOB})$, even if slightly smaller than in the local case, are greater than 95 percent: this model is a good model too.

Note that this *global model* is a special case of the previous local model. Here we have the same intercept e_0, which has been forced to be the same as in the local fitting, and we have constrained the three k_θ to be the same and equal to k. Thus, as we have fitted the same data with the same model, but with a reduced number of parameters, the global fitting is expected to produce a worse fit (in the χ^2 sense) than the local one. In fact, what we are really interested in is to understand whether that global model, that hypothesize the independence of masking on noise sector width, is *statistically* equivalent to the local one. If this is the case, we have no reason to reject the linear, global model: if the *goodness* of the fit is not influenced by the fact of estimating one k instead of three k_θ, this means

that the variation of sector half width θ does not influence the trend of the results, thus a linear broadband mechanism must mediate the detection.

To verify if the global model is statistically equivalent to the local one, a statistical test is required. We have used a special *likelihood ratio test* to solve this *nested fitting problem.*

5.3.3 Nested Fitting

Let us assume that the same set of experimental data was fit to two different fitting models or equations, one of which is a simpler case of the other. Very often a fitting model with more adjustable parameters will produce a better fit (in the χ^2 sense) than an alternative model with fewer adjustable parameters. In fact, the question is whether the decrease in the sum of squares with the increase in number of parameters is statistically significant. This is a typical *nested fitting problem.*

We had a model, what we have called *local model*, that fitted well the data. Then, we had another reduced model, the *global model*, that forced the three values k_θ to be the same and that fitted the experimental data well, but not as well as the local one. To demonstrate that the hypothesis of linearity is correct, we had to show that the two models, one of which is a reduced (*nested*) case of the other, are statistically equivalent. We had thus to face a nested fitting problem. This problem can be solved using a *likelihood ratio test* [65].

Likelihood Ratio Tests

Suppose that a variable X has a *density function* $f(x; p_1, ..., p_m)$ that depends on m parameters. The density function of a random variable X is that function f defined by $f(x) = P(X = x)$. Suppose that n observations are to be made of the variable X. Let $X_1, X_2, ..., Xn$ denote the random variables corresponding to these n observations. Then the function given by:

$$L(x_1, ..., x_n; p_1, ..., p_m) = \prod_{i=1}^{n} f(x_i; p) \tag{5.7}$$

defines a function of the random sample values $x_1, ..., x_n$ and of the parameters $p_1, ..., p_m$ which is known as the *likelihood function of the sample.*

Now, let the hypothesis to be tested be denoted by $H_0 : p_i = p'_i (i = 1, 2, ...m)$, where p'_i may or may not denote a numerical value. Thus, if there are two parameters, H_0 might be the hypothesis that $p_1 = 15$ with p_2 unspecified; then $p'_1 = 15$ and $p'_2 = p_2$.

Let $\widehat{p_i}$ denote the estimate of the parameter p_i and $\widehat{p'_i}$ denote the estimate of p_i when H_0 is true. Now, one can form the ratio:

$$\lambda = \frac{L(X, \widehat{p'})}{L(X, \widehat{p})} \tag{5.8}$$

with $L(X,p) = \prod_{i=1}^{n} f(X_i; p_1, ..., p_m)$, where X represents the vector $X_1, X_2, ..., X_n$ and where the likelihood function is treated as a function of the parameters and of the random variables $X_1, X_2, ..., X_n$. Thus, λ is the ratio of two likelihood functions when their parameters have been replaced by their estimators.

Since the estimators $\widehat{p_i}$ and $\widehat{p_i'}$ are functions of the random variables $X_1, X_2, ..., X_n$, the ratio λ is a function of $X_1, X_2, ..., X_n$ only and is therefore an observable random variable, that is, a statistic.

The denominator of λ is the likelihood function calculated considering all the parameters, whereas the numerator is the function computed only after some of the parameters have been restricted by H_0. Thus, it is clear that the numerator cannot exceed the denominator in value and therefore that λ can assume values between 0 and 1 only. The value of the likelihood function gives the probability of the sample point $x_1, x_2, ..., x_n$. Therefore, if λ has a value close to 1, it follows that the probability of the sample point could not be increased much by allowing the parameters to assume values other than those possible under H_0; consequently, a value of λ near 1 corresponds intuitively to considerable belief in the reasonableness of the hypothesis H_0. If, on the other hand, the value of λ is close to 0, it implies that the probability of the sample point is very low under the hypothesis H_0 as contrasted to its value under certain other values of the parameters not permitted under H_0. Therefore, a value of λ near 0 corresponds to considerable belief in the unreasonableness of the hypothesis.

Now suppose that H_0 is true and the density function of the random variable λ, say $g(\lambda)$, has been found. This is theoretically possible if the explicit form of $f(x; p_1', ..., p_m')$ is known. Suppose, further, that $g(\lambda)$ does not depend on any unknown parameters. Then, since small values of λ should lead to reject the hypothesis H_0, one finds the value of λ, call it λ_0, such that:

$$\int_0^{\lambda_0} g(\lambda) d\lambda = \alpha \tag{5.9}$$

where α is the probability of rejecting H_0 when H_0 is true. A conventional value for α is $\alpha = 0.05$; this means that approximately 5 percent of the time true hypothesis being tested will be rejected.

The *critical region* of size α for testing H_0 by means of the statistic λ is therefore chosen to be the interval $0 \leq \lambda \leq \lambda_0$.

Thus, the construction of a likelihood test can be summarized as follows [65].

LIKELIHOOD RATIO TESTS: To test a hypothesis H_0 simple or composite, use the statistic λ given by eq. 5.8 and reject H_0 if, and only if, the sample value of λ satisfies the inequality $0 \leq \lambda \leq \lambda_0$, where λ is given by eq. 5.9.

For large samples, that is for large values of n, there is a good approximation to the distribution of λ which eliminates the necessity of finding its exact distribution. This result from the advanced theory of statistics can be expressed in the form of a theorem [65]:

Theorem 5.3.3.1 *Under certain regularity conditions, when the hypothesis H_0 is true, the random variable $-2\log_e \lambda$, where λ is given by eq. 5.8, has a distribution that approaches that of a χ^2 variable as n becomes infinite, with its degrees of freedom equal to the number of parameters that are determined by the hypothesis H_0.*

Since small values of λ correspond to large values of $-2\log_e \lambda$, it follows that the critical region for a test based on the quantity $-2\log_e \lambda$ will consist of large values of this variable. If the borderline of a critical region for the χ^2 variable $-2\log_e \lambda$ is denoted by χ_0^2, then χ_0^2 must be a number such that $P_d(\chi^2 > \chi_0^2) = \alpha$. Thus, in order to determine the critical region for this approximate likelihood ratio test, it suffices to find a critical value of χ^2 using eq. 5.5.

Application of the Method to Our Experiment

What we want to understand is whether the global model, that hypothesizes the independence of masking on noise sector width, is statistically equivalent to the local one. To do that we have used a likelihood ratio test applied to that nested fitting problem. If the goodness of the fit is not influenced by the fact that one estimates one parameter k instead of three values k_θ, this means that the variation of sector width does not influence the behavior of the mechanism mediating the detection.

Let assume that the observed data are distributed around their expected values according to a Gaussian distribution, that is, with a density function:

$$f(x,p) = \frac{e^{-\frac{1}{2}\left(\frac{x-\mu(p)}{\sigma}\right)^2}}{\sqrt{2\pi\sigma^2}} \tag{5.10}$$

where $\mu(p)$ is the expected value from the model and depends on the parameters of the model and σ is the standard deviation of the observed point.

For this problem the sample value of the likelihood function is:

$$L(x,p) = \prod_{i=1}^{n} (2\pi\sigma_i^2)^{-\frac{1}{2}} e^{-\frac{1}{2}\left(\frac{x_i-\mu(p)}{\sigma_i}\right)^2} \tag{5.11}$$

where n is the dimension of the sample.

Now, let us indicate the expected value computed according to the local model, that is estimating three values k_θ, with $\mu(\theta)$. Similarly, we indicate the value expected from the global model, e.g. forcing the three values k_θ to be the same, as μ'. Thus, the hypothesis to test here is $H_0 : \mu(\theta = 0) = \mu(\theta = 30) = \mu(\theta = 60) = \mu'$.

Thus, one can write the likelihood function under the global conditions as:

$$L(x,\widehat{p}) = \prod_{i=1}^{n} (2\pi\sigma_i^2)^{-\frac{1}{2}} e^{-\frac{1}{2}\left(\frac{x_i-\mu_i(\theta)}{\sigma_i}\right)^2} \tag{5.12}$$

because $\widehat{p} : \mu(\widehat{p}) = \mu_i(\theta)$. Note that the expected value in this case can vary from one point to another.

Under the hypothesis H_0, one can write the likelihood function as:

$$L(x, \widehat{p'}) = \prod_{i=1}^{n} (2\pi\sigma_i^2)^{-\frac{1}{2}} e^{-\frac{1}{2}\left(\frac{x_i-\mu'}{\sigma_i}\right)^2} \tag{5.13}$$

being $\widehat{p'} : \mu(\widehat{p'}) = \mu'$.
Thus λ, as given by eq. 5.8 for a set of sample values, becomes:

$$\lambda = \frac{\prod_{i=1}^{n} (2\pi\sigma_i^2)^{-\frac{1}{2}} e^{-\frac{1}{2}\left(\frac{x_i-\mu'}{\sigma_i}\right)^2}}{\prod_{i=1}^{n} (2\pi\sigma_i^2)^{-\frac{1}{2}} e^{-\frac{1}{2}\left(\frac{x_i-\mu_i(\theta)}{\sigma_i}\right)^2}} \tag{5.14}$$

This is equivalent to:

$$\lambda = \frac{\prod_{i=1}^{n} e^{-\frac{1}{2}(\frac{x_i-\mu'}{\sigma_i})^2}}{\prod_{i=1}^{n} e^{-\frac{1}{2}\left(\frac{x_i-\mu_i(\theta)}{\sigma_i}\right)^2}} \tag{5.15}$$

Now, calculating $-2\log_e \lambda$, we obtain:

$$-2\log_e \lambda = \sum_{i=1}^{n} \left(\frac{x_i - \mu'}{\sigma_i}\right)^2 - \sum_{i=1}^{n} \left(\frac{x_i - \mu_i(\theta)}{\sigma_i}\right)^2 \tag{5.16}$$

The two summations on the right side of eq. 5.16 represent two χ^2 values. More precisely, they are the two χ^2 quantities calculated using eq. 5.3, in the local and global cases respectively. Thus, calling the χ^2 variable $-2\log_e \lambda$, χ^2_{DIFF}, we can write:

$$\chi^2_{DIFF} = \chi^2_{GLOB} - \chi^2_{LOC} \tag{5.17}$$

where χ^2_{GLOB} and χ^2_{LOC} are the two χ^2 values calculated for the global and local case respectively.

Thus, we can calculate χ^2_{GLOB} and χ^2_{LOC} as shown in sec. 3.2. Then the difference between those two quantities is computed: the result, from eq. 5.17, is a χ^2 variable again. The degrees of freedom of this variable, from theorem 5.3.3.1, are equal to the number of parameters that are determined by the hypothesis H_0. In our case, the hypothesis H_0 constrains the three values of k_θ to be the same and equal to a common value k, that is, reduces the number of parameters from four to two. Consequently, the number of degrees of freedom of the χ^2 variable χ^2_{DIFF} are $d = 2$. At this point, we can calculate $P_2(\chi^2 \geq \chi^2_{DIFF})$ using eq. 5.5; if the value is large (typically greater than 5 percent), the hypothesized reduced model cannot be rejected.

5.3.4 Results and Discussion

In table 1, the χ^2 statistics for four observers (IO, PG, ES, GM) are summarized. These statistics result from the data of three series of experiments.

Subject	Color Azimuth ϕ in degrees	χ^2_{LOC}	χ^2_{GLOB}	χ^2_{DIFF}	$P_2(\chi^2 \geq \chi^2_{DIFF})$
IO	0	0.0735	0.0884	0.0149	0.9926
	15	0.151	0.19	0.039	0.9807
	75	0.4136	0.6499	0.2363	0.8886
	90	0.85	2.4053	1.5552	0.4595
PG*	0	0.0602	0.0898	0.0296	0.9853
	15	0.0269	0.0757	0.0488	0.9759
	75	0.1661	0.2012	0.0351	0.9826
	90	0.5618	0.9636	0.4018	0.818
ES*	0	0.0753	0.1197	0.0443	0.9781
	15	0.0865	0.1328	0.0463	0.9771
	75	0.6187	0.8179	0.1992	0.9052
	90	0.3858	0.4519	0.0661	0.9675
GM	0	0.1743	0.2496	0.0752	0.9631
	15	0.2682	0.4903	0.2221	0.8949
	75	0.1639	1.3589	1.195	0.5502
	90	0.2093	1.3397	1.1304	0.5682

Table 5.1: Summary of χ^2 statistics for subjects IO, PG, ES and GM. Results for three series of experiments.* PG and ES result to be "superior discriminators" from Farnsworth Munsell 100-hue test.

The complete set of statistics are collected in Appendix B.
Several considerations can be done analyzing these data.

- All the probabilities $P_2(\chi^2 \geq \chi^2_{DIFF})$ calculated for different chromatic directions in the equiluminant plane of the DKL color space and for different observers are quite large. This strongly suggests that the tested hypothesis H_0 of a linear mechanism mediating chromatic detection is highly reliable.

  Developing our statistics, we have made two main assumptions: the measured data are distributed around their expected values following a Gaussian distribution and the statistic $-2\log_e \lambda$ is a χ^2 variable. The first assumption is justified when the number of measurements is reasonably large (typically about 5) [64], thus our three measures could be a few quantity to make the assumption of normally distributed data.

  The hypothesis of $-2\log_e \lambda$ being a χ^2 variable derives from the theorem 5.3.3.1 and is justified when the number of considered points n becomes infinite. This is of course an approximation, but the approximate likelihood ratio test is largely employed since there is no assurance that the variable λ could be related to a familiar variable. Thus, the greater the number of considered point n is, the more reliable the approximate test will be. In this case too, we do not have a very large set of points on which the

model was built. However, these two approximations seem to be balanced by the considerably high values of the probabilities $P_2(\chi^2 \geq \chi^2_{DIFF})$; the linear hypothesis still appears to be considerably reasonable.

- Since these results hold true for different directions in the color space, including both cardinal directions and intermediate directions, it seems reasonable to argue that human visual system has higher order chromatic mechanisms tuned to *any* direction in the chromatic space. Moreover, these mechanisms should combine cone signals linearly, as can be deduced from the fact that the human chromatic sensitivity is not influenced by the amplitude of the noise sector.

- The independence of human chromatic sensitivities on the noise sector width suggests that the performances on color detection tasks are not influenced by the particular hues present in the mask, but only by the saturation of the masking colors, that is related to the amplitude n of the sectored noise. If this is the case, the detection of a color within a spatial chromatic noise would be independent on the chromaticities of the noise and would only depend on the intensity of such a noise. This aspect could be of great interest for applications in the field of digital imaging.

- Our results agree with the findings of D'Zmura and Knoblauch [3] in the temporal domain. In their study, they found evidences for the existence of linear chromatic detection mechanisms oriented along the four color directions tested (red, orange, yellow and violet). Also the results from visual search studies of D'Zmura [6] suggest that the human visual system possesses chromatic linear higher order mechanisms tuned to intermediate directions. Moreover, our data agree with the evidences shown by Krauskopf and colleagues [4, 5] in their habituation studies, where they found strong evidences for the presence of higher order, intermediate chromatic mechanisms mediating human perception.

- Even if nonlinear mechanisms models (case 2 in sec. 4.5.2) and two mechanisms models (case 3 in sec. 4.5.2) have not been quantitatively described and analyzed, our results point to a rejection of those two alternative models. Moreover, even a qualitative analysis of the data does not seem to suggest any indication in those two directions.

- There is a clear difference between the performances of *superior* and *average discriminators* (see sec. 4.6). The data measured for superior discriminators (ES and PG) fit better the model, especially when the color azimuth ϕ approaches the direction $\phi = 90°$ that indicates a yellow hue. Note that none of the two average subjects has any particular problem in discriminating yellowish hues. Moreover, the results are more stable; the values of $P_2(\chi^2 \geq \chi^2_{DIFF})$ are always quite high. Thus, performances in color detection seem to be influenced by the discrimination skills of the subject, especially when the test color tends to yellowish hues.

In summary, the results for the detection of spatial chromatic Gaussian blobs within a sectored noise mask do not depend on sector half width. This holds true for all the tested colors (two nuances of red, orange and yellow) and for all the observers. These results agree with the findings of D'Zmura and Knoblauch [3] in the temporal domain, with the evidences shown by Krauskopf and colleagues [4, 5] in their habituation studies and with the visual search studies of D'Zmura [6].

Such results strongly suggest that the human visual system mediates the detection of chromatic spatial signals through linear, broadband detection mechanisms tuned to the directions of the color space tested. The tested signal directions include two that were expected to isolate classical color-opponent mechanisms, that is, the yellow and the red mechanisms. In addiction, we have tested two intermediate directions, orange and reddish. Thus, the results are consistent with the presence of chromatic detection mechanisms sensible to the tested color and that combine the cone signals in a linear fashion.

5.4 Conclusions

This chapter has been dedicated to the presentation of the methods used to interpret the psychophysical data collected in our tests and and to the presentation of the result of such analysis.

In the first sections, the methods used to measure the thresholds and to plot them have been exposed. This was a necessary step to correctly interpret the experimental data. In section 3, the noise masking model used to fit the results was presented and the fitting to the data under two different hypotheses exposed. The results of such fitting procedures were compared using a particular likelihood ratio test. The theoretical basis of such an analysis and the results have been exposed and discussed.

Chapter 6

Conclusions

6.1 Summary of Achievements

In this chapter we review the most important issues and contributions presented in this report. We also propose some directions for possible extensions of the presented work.

In this project, a psychophysical approach to higher order chromatic mechanisms has been investigated. The objective of this investigation is to better understand the mechanisms that control the detection of chromatic spatial distributions, in order to provide a model for the representation of chromatic spatial information.

The perception of spatial chromatic patterns - simple two-color images, textures or natural images - has been investigated to try to understand the mechanisms that such an experience involves. When looking at a colored scene, lots of higher order mechanisms take part to perception. Such mechanisms can be seen as a way to model how the human brain process the visual information.

To characterize the mechanisms that the human visual system employs, we have set up a psychophysical experiment. In doing that, we have been inspired by the study of 1998 of D'Zmura and Knoblauch [3]. They investigated the detection chromatic mechanisms in the temporal domain; we have transduced their paradigm in the spatial domain. Threshold measurements have been performed to estimate the behavior of visual system in color detection tasks. Such measurements have been effected using a staircase procedure and a two alternative forced choice method. The goal of our threshold experiments was to express this detection limit as a function of the noise properties and thus to characterize the mechanisms involved in these color detection operations. To do that a sectored noise masking technique has been used. Sectored noise samples are randomly chosen from a sector of variable width defined in the equiluminant plane of the DKL color space. These samples define the chromaticities of a noise mask that is superimposed to a monochromatic test signal, consisting on a spatially isotropic Gaussian blob. The signal and the noise sector lie along the same chromatic axis in the DKL color space. Using this masking technique, it has been possible to determine whether color detection mechanisms combine the cones signals in a linear or nonlinear fashion, by measuring the variation of the human visual

system performances with the variation of noise sector width. In fact, a linear mechanism tuned to a certain color direction can be represented as a vector in the DKL color space and its response to a stimulation as the dot product between the vectors representing the mechanism and the stimulus. Thus, a linear mechanism is not influenced by any stimulation component orthogonal to its direction. Since sectored noise is always oriented along the signal axis, the variation of its width involves a variation of only the noise components orthogonal to the signal chromatic direction. Thus, the sensitivity of a linear mechanism are not influenced by the variation of noise sector width. On the other hand, the performances of a nonlinear mechanism should be affected by the increasing or decreasing of noise sector width.

To interpret the data, we have fitted the thresholds measured varying noise sector width and amplitude and color test direction, to a noise masking regular model proposed by Pelli [62] and Legge et al. [63]. The fits were calculated under two different hypotheses on the behavior of the mechanisms mediating color detection. We have first estimated a general model and then a reduced version of such a model, that was forced to respect the hypothesis of linearity, has been computed. The results of those two fittings have been compared using a special version of the *likelihood ratio test*. This procedure is called *nested fitting technique*.

The results obtained show that the hypothesized linear model succeeds in representing the data resulting from our tests with sectored noise masking. The human visual system seems to mediate the detection of chromatic spatial patterns through linear, broadband detection mechanisms tuned to the directions of the color space tested. These results agree with the findings of several recent studies in the field of vision research, confirming therefore the results of the study of D'Zmura and Knoblauch [3] obtained in the temporal domain. Another interesting result is that the performances in our color detection tasks depend on chromatic discrimination skills of the subjects.

6.2 Future Works

The work presented in this report can be improved and extended in several ways.

- More tests could be performed in order to have more precise and reliable statistics. We have discussed in section 4.3.3 the approximations and assumptions we have done to develop our analysis. They are all based on the fact of considering a large number of tests and a large number of data points. Thus, it would be preferable to make more series of experiments (at least 5, as suggested by Taylor [64]) and to test more noise levels, in order to evaluate the model basing the analysis on a larger set of points.

  Moreover, a larger number of chromatic directions should be tested, in order to confirm the deduction that human visual system possess chromatic detection mechanisms tuned to *any* direction of the color space.

- A comparison with alternative higher order mechanism models could be effected. In order to better understand the behavior of human visual system, one should compare the performances of the hypothesized linear model with the alternative nonlinear and two-cardinal-directions models. In section 4.5.2 we have intuitively presented those two models, but a deeper *quantitative* analysis is required.

- Tests with a more precise video card have to be done. A VSG 15-bit video card is recently available in the laboratory; such a video board could allow more precise threshold measurements. The fact of using a standard 8-bit card could influence the measures, especially in the no noise condition, when the signal is tested on the uniform grey background. In this condition, the human visual system seems to be quite sensible to chromatic contrast and thus the 8-bit quantization could be rough.

- Exploitability for chromatic noise masking, perceptual image quality metrics, watermarking, image compression. A deeper knowledge of how the human visual system processes chromatic spatial information would allow to develop more performing applications. Moreover, the characterization of noise masking effects on the perception of spatial distributions of color would be of great interest for gamut mapping applications.

APPENDIX

Appendix A

Monitor Calibration and Characterization

A.1 Calibration

The procedure used to characterize the monitor employed for the psychophysical experiments is described in this section.

In order to control as much as possible the performances of the apparatus, we have measured the phosphors characteristics of the monitor with the Minolta CS-1000 spectroradiometer. This machine measures the spectral response every 1 nm in the range 380 nm-780 nm in watts per steradian (W/st). The screen is a Barco PCD 321 Plus 21" driven by a Matrox G450 graphic card and set to a resolution of 1280×1024 pixel.

The stimuli used to make the measurements were square patches, which were displayed in the center of the screen in a completely dark room. We have measured three sets of colored patches, *red*, *green* and *blue*, for color numbers varying between 15 and 255 with a step of 15, that is, 17 measures have been taken for each color. Moreover, *grey* patches have been measured in the range 0-255, taking thus 18 measurements. For example, a color number of 255 for the red patch corresponds to a stimulation: [255 0 0]; this value corresponds to the most saturated *red* that the monitor can display. Thus, a grey number equal to 0 represents the monitor stimulation value [0 0 0], corresponding to the *black* of the screen, while a grey number of 255 corresponds to the stimulation [255 255 255], that indicates the *reference white*.

The measurements have been done using a C program developed in the laboratory. This program allows an automatic synchronization between the displaying of the stimulus on the screen and the measure of the Minolta spectroradiometer. The measured spectra are shown in fig. A.1.

Using such measures, we have estimated the *gamma*(γ)-function (see section 4.8.1) for each gun red, green and blue. We have calculated the luminance values Y_k^R, Y_k^G, Y_k^B ($k = 1, ..., 18$) for the three channels and for each stimulus. The gamma functions have been computed for normalized values of the stimulation and of the luminance. Thus,

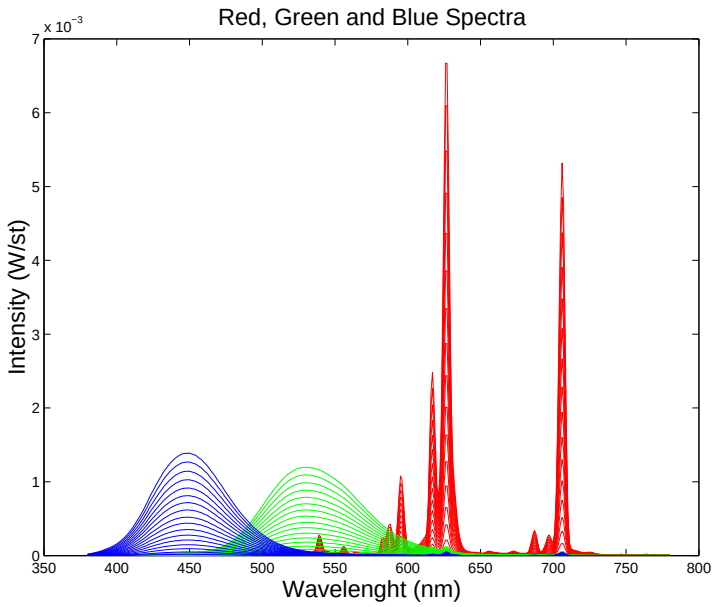

Figure A.1: Measured spectra for the Barco PCD 321 Plus display. The measures have been effectuated with a Minolta CS-1000 spectroradiometer.

the stimulus values were $s_k = [15(k-1)/255]$ and the luminance values $\widetilde{Y_k^R} = Y_k^R/Y_{18}^R$, $\widetilde{Y_k^G} = Y_k^G/Y_{18}^G$, $\widetilde{Y_k^B} = Y_k^B/Y_{18}^B$, where Y_{18}^i $(i = R, G, B)$ was the luminance value of the most intense patch for each hue. Thus, we had to estimate the γ-functions for the three channels, γ_R, γ_G and γ_B, as:

$$\begin{aligned} \widetilde{Y_k^R} &= (a_R + b_R s_k)^{\gamma_R} \\ \widetilde{Y_k^G} &= (a_G + b_G s_k)^{\gamma_G} \\ \widetilde{Y_k^B} &= (a_B + b_B s_k)^{\gamma_B} \end{aligned} \tag{A.1}$$

We have found the parameters a_i, b_i, γ_i $(i = R, G, B)$ that satisfy these equations using the Matlab function *lsqcurvefit* that solves nonlinear equations in the least square sense. The values of the parameters a_i, b_i, γ_i are resumed in table A.1.

	γ	a	b
Red Channel	1.5886	2.2233e-014	1.0018
Green Channel	1.5335	2.2204e-014	1.0009
Blue Channel	1.5316	2.2204e-014	0.99997

Table A.1: The values of the parameters a, b, γ estimated for the three guns.

Now, a color C represented in normalized RGB coordinates as $C = [r, g, b]$ can be *linearized* as:

$$C_{LIN} = [(r^{1/\gamma_R} - a_R)/b_R, (g^{1/\gamma_G} - a_G)/b_G, (b^{1/\gamma_B} - a_B)/b_B] \tag{A.2}$$

where now C_{LIN} is the stimulation that one should give to the screen to obtain stimuli linear in luminance.

A.2 Characterization

Once the display has been *calibrated*, one can *characterize* it, finding a conversion matrix from its proper RGB linearized coordinates to a known color space. In our case, we have considered the CIE 1964 10° color space, as the stimuli utilized for our experiments are about 10° of visual angle wide. A simple transformation from linear RGB to 1964 XYZ is as follow:

$$\mathbf{S} \approx \mathbf{PT} \tag{A.3}$$

where $\mathbf{P}$ (52×3) are the normalized RGB values of all the measured patches (17 red, 17 green, 17 blue and 18 grey), $\mathbf{S}$ (52×3) are the correspondent 1964 XYZ values and $\mathbf{T}$ is a 3×3 matrix. The matrix $\mathbf{T}$ that best maps $\mathbf{P}$ to $\mathbf{S}$ minimizing least square error is computed using the Moore-Penrose inverse [59]:

$$\mathbf{T} = (\mathbf{P}^T\mathbf{P})^{-1}\mathbf{P}^T\mathbf{S} \tag{A.4}$$

The estimated matrix $\mathbf{T}$ is:

$$\mathbf{T} = \begin{bmatrix} 36.759 & 20.418 & 2.4482 \\ 27.686 & 51.59 & 7.7836 \\ 15.799 & 9.9176 & 83.152 \end{bmatrix} \tag{A.5}$$

Now one can directly map a color defined in every color space into RGB linear values of the monitor passing through the 1964 XYZ color coordinates and using the matrix $\mathbf{T}$. In our case, we had defined our stimuli in the DKL color space which is related to the LMS opponent color space by a linear relation, that is a 3×3 matrix [33], called $\mathbf{A}$, that is expressed by eq. 2.9. The LMS color coordinates we have employed are those based on the cone fundamentals measured by Stockman et al. in 1993 [60]. Those coordinates can be related to the CIE 1964 XYZ color space by an approximate linear relationship assuming that the S cones make no contribution to vision for wavelengths greater than 525nm [60]. Such 3×3 matrix, let us call it $\mathbf{B}$, that transforms LMS into CIE 1964 XYZ coordinates, was found to be:

$$\mathbf{B} = \begin{bmatrix} 1.8781 & -1.2818 & 0.4095 \\ 0.6722 & 0.3682 & -0.0049 \\ -0.0186 & 0.0336 & 2.0275 \end{bmatrix} \tag{A.6}$$

The procedure that relates the DKL color space to the RGB of the monitor so that the displayed colors are linear in luminance is diagrammed in fig. A.2.

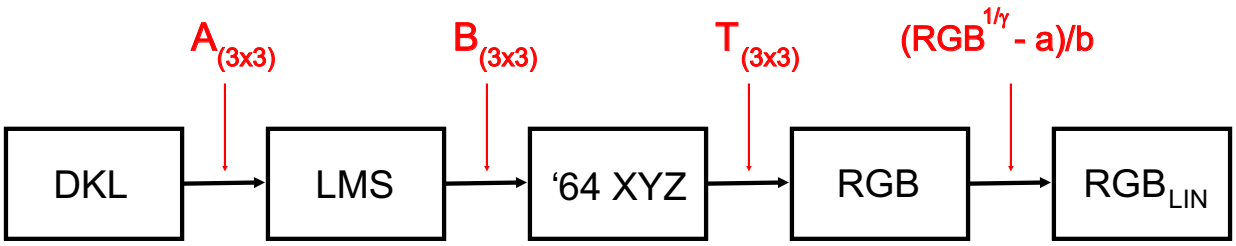

Figure A.2: Diagram of the procedure employed to relate the DKL color space to the monitor RGB coordinates.

Appendix B

Results

In this section, we present the complete set of statistics derived from our experiments.

The data shown in table B.1 come from three series of experiments, except for subject NP, whose statistics have been computed on the basis of two series. The experiments were performed by four female subjects (ES, PG, GM and ED) and two male observers (IO and NP). Two of them (ES and PG) result to be "superior discriminators" from Farnsworth Munsell 100-hue test (see sec. 4.6).

Four subjects (IO, PG, ES and GM) tested the four color directions indicated by azimuths $\phi = 0°$, $\phi = 15°$, $\phi = 75°$, $\phi = 90°$ and corresponding to red, light reddish, orange and yellow signals respectively. Observers ED and NP performed reduced series of experiments, testing three directions in the color space; ED has not tested the orange signal corresponding to the direction $\phi = 75°$ while NP has not performed tests with the reddish color direction indicated by $\phi = 15°$.

Subject	Color Azimuth ϕ in degrees	χ^2_{LOC}	χ^2_{GLOB}	χ^2_{DIFF}	$P_2(\chi^2 \geq \chi^2_{DIFF})$
IO	0	0.0735	0.0884	0.0149	0.9926
	15	0.151	0.19	0.039	0.9807
	75	0.4136	0.6499	0.2363	0.8886
	90	0.85	2.4053	1.5552	0.4595
PG*	0	0.0602	0.0898	0.0296	0.9853
	15	0.0269	0.0757	0.0488	0.9759
	75	0.1661	0.2012	0.0351	0.9826
	90	0.5618	0.9636	0.4018	0.818
ES*	0	0.0753	0.1197	0.0443	0.9781
	15	0.0865	0.1328	0.0463	0.9771
	75	0.6187	0.8179	0.1992	0.9052
	90	0.3858	0.4519	0.0661	0.9675
GM	0	0.1743	0.2496	0.0752	0.9631
	15	0.2682	0.4903	0.2221	0.8949
	75	0.1639	1.3589	1.195	0.5502
	90	0.2093	1.3397	1.1304	0.5682
ED	0	0.0796	0.1312	0.0516	0.9745
	15	0.0846	0.1203	0.0357	0.9823
	90	0.5074	0.8456	0.3383	0.8444
NP	0	0.1481	0.2576	0.1095	0.9467
	75	1.0639	2.1639	1.1016	0.5765
	90	0.1481	0.2576	0.1095	0.9467

Table B.1: Summary of χ^2 statistics for subjects IO, PG, ES, GM, ED and NP. Results for three series of experiments, except for observer NP (two series).* PG and ES result to be "superior discriminators" from Farnsworth Munsell 100-hue test.

Bibliography

[1] J. Guild. The colorimetric properties of the spectrum. *Philosophical Transactions of the Royal Society of London*, (A230):149–187, 1931.

[2] W.D. Wright. A re-determination of the trichromatic coefficients of the spectral colours. *Transactions of the Optical Society*, (30):141–164, 1928.

[3] M. D'Zmura and K. Knoblauch. Spectral bandwidths for the detection of color. *Vision Research*, 38:3117–3128, 1998.

[4] D.R. Williams J. Krauskopf and D.W. Heeley. Cardinal directions of color space. *Vision Research*, 22:1123–1131, 1982.

[5] M.B. Mandler J. Krauskopf, D.R. Williams and A.M. Brown. Higher order color mechanisms. *Vision Research*, 26(1):23–32, 1986.

[6] M. D'Zmura. Color in visual search. *Vision Research*, 31(6):951–966, 1991.

[7] K.R. Gegenfurtner and D.C. Kiper. Contrast detection in luminance and chromatic noise. *J. Opt. Soc. Am. A*, 9(11):1880–1888, Nov 1992.

[8] M.A. Webster and J.D. Mollon. The influence of contrast adaptation on color appearance. *Vision Research*, 34(15):1993–2020, Aug 1994.

[9] A. Stockman and L.T. Sharpe. The spectral sensitivities of the middle- and long-wavelength-sensitive cones derived from measurements in observers of known genotype. *Vision Research*, (40):1711–1737, 2000.

[10] W. S. Stiles and J.M. Burch. Npl colour-matching investigation: final report. *Optica Acta*, (6):1–26, 1959.

[11] L.T. Sharpe A. Stockman and C.C. Fach. The spectral sensitivity of the human short-wavelength cones. *Vision Research*, (39):2901–2927, 1999.

[12] M.D. Fairchild. *Color appearence models*. Addison-Wesley, 1998.

[13] H. Helmholtz. *Physiological Optics*. Optical Society of America, [1866]1924.

[14] T. Young. On the theory of light and colors. *Philosophical Transactions of the Royal Society*, (91):12–49, 1902.

[15] J.C. Maxwell. On the theory of three primary colors. *Proc. Roy Inst.*, (3):370–375, 1858-1862.

[16] E. Hering. *Outlines of a theory of the light sense.* Harvard University Press, Cambridge, Mass., 1920.

[17] D. Jameson and L.M. Hurvich. Some quantitative aspects of an opponent-colors theory: I. chromatic responses and spectral saturation. *J. Opt. Soc. Am.*, (45):546–552, 1955.

[18] S.T. Kitai R.L. DeValois, C.J. Smith and S.J. Karoly. Responses of single cells in different layers of the primate lateral geniculate nucleus to monochromatic light. *Science*, (127):238–239, 1958.

[19] H. Grassmann. On the theory of compound colors. *Edimb. Dublin Philos. Mag. J. Sci.*, 7(4):254–264, 1854.

[20] Commission Internationale de l'Eclairage. Commission internationale de l'eclairage proceedings. Cambridge, 1932.

[21] Commission Internationale de l'Eclairage. Committee report e-1.4.1. In *CIE Proceedings (1964) Vienna Session*, volume B, pages 209–220, Bureau Central de la CIE, Paris, 1963.

[22] B.D. Judd. Report of u.s. secretariat committee on colorimetry and artificial daylight. In *Proceedings of the Twelfth Session of the CIE, Stockholm*, volume 1, page 11, Paris: Bureau Central de la CIE, 1932.

[23] J.J. Vos. Colorimetric and photometric properties of a 2-deg fundamental observer. *Color Research and Application*, (3):125–128, 1978.

[24] V.C. Smith and J. Pokorny. Spectral sensitivity of the foveal cone photopigments between 400 and 500 nm. *Vision Research*, (15):161–171, 1975.

[25] Commission Internationale de l'Eclairage. No. 15.2. In *Colorimetry, 2nd ed.*, volume 1, page 11, Vienna, Austria, 1976.

[26] J. Krauskopf A.M. Derrington and P. Lennie. Chromatic mechanisms in lateral geniculate nucleus of macaque. *J. Physiol. Lond.*, (357):241–265, 1984.

[27] D.I.A. MacLeod and R.M. Boynton. Chromaticity diagram showing cone excitation by stimuli of equal luminance. *J. Opt. Soc. Am.*, 69:1183–1186, 1979.

[28] D. Brainard. *Human Color Vision*, chapter : Cone contrast and opponent modulation color spaces, pages 563–579. P. Kaiser and R.M. Boynton, Optical Society of America; Washington, DC, 1996.

[29] G.T. Fechner. *Elemets of psychophysics Vol.1.* Holt,Rinehart and Winston, New York, [1860]1966.

[30] S.S. Stevens. To honor fechner and repeal his law. *Science*, (133):80–86, 1961.

[31] P. Haubner H. Bodmann and A. Marsden. A unified relationship between brightness and luminance. In *CIE Proceedings Kyoto Session 1979*, pages 99–102, CIE Central Bureau, Paris, 1980.

[32] M.H. Pirenne. *The Eye, vol 2*, chapter : Adaptation and Night Vision. H. Davson ed., London, Academic Press, 1962.

[33] D.H. Brainard and B.A. Wandell. Asymmetric color matching: how color appearance depends on the illuminant. *J. Opt. Soc. Am. A*, (9):1433–1448, 1992.

[34] Leonardo da Vinci. *Treatise on Painting*. Princeton University Press, [1492]1956.

[35] M.E. Chevreul. *The Law of Contrast of Colors and Their Application to Arts*. G. Routledge, [1845]1868.

[36] R.M. Evans. *An Introduction to color*. John Wiley & Sons, 1948.

[37] J. Alberts. *Interaction of Color*. Yale University Press, 1963.

[38] L.M. Hurvich. *Color Vision*. Sinauer Associates, 1981.

[39] R.M. Boynton. *Human Color Vision*. Optical Society of America, 1979.

[40] J. von Kries. *Chromatic Adaptation*. MacAdam DL. MIT Press, [1905]1970.

[41] P. Whittle. *The psychophysics of contrast brightness*. Lawrence Erlbaum, 1994.

[42] L. M. Hurvich and D. Jameson. Opponent chromatic induction: Experimental evaluation and theoretical account. *J. Opt. Soc. Am.*, 51:46–53, 1961.

[43] J. Walraven. Spatial characteristics of chromatic induction; the segregation of lateral effects from stray light artefacts. *Vision Research*, 13:1739–1753, 1973.

[44] M. Wesner and S. K. Shevell. Color perception within chromatic context: Changes in red/green equilibria caused by noncontiguous light. *Vision Research*, 32:1623–1634, 1992.

[45] S. K. Shevell and J. Wei. Chromatic induction: Border contrast or adaptation to surrounding light? *Vision Research*, 38:1561–1566, 1998.

[46] T. D. Albright T. Wachtler and T. J. Sejnowski. Nonlocal interactions in color perception: Nonlinear processing of chromatic signals from remote inducers. *Vision Research*, 41:1535–1546, 2001.

[47] J. Wei C. S. Barnes and S. K. Shevell. Chromatic induction with remote chromatic contrast varied in magnitude, spatial frequency and chromaticity. *Vision Research*, 39:3561–3574, 1999.

[48] J. W. Jenness and S. K. Shevell. Color appearance with sparse chromatic contrast. *Vision Research*, 35:797–805, 1995.

[49] R. O. Brown and D. I. A. MacLeod. Color appearance depends on the variance of surround colors. *Current Biology*, 7:844–849, 1997.

[50] P.G. Engeldrum. *Psychometric scaling.* Imcotek Press, Winchester,Massachussets,USA, 2000.

[51] F. Giulianini and R.T. Eskew Jr. Chromatic masking in the (δl/l, δm/m) plane of cone-contrast space reveals only two direction mechanisms. *Vision Research*, 38:3913–3926, 1998.

[52] J.R. Newton R.T. Eskew Jr and F. Giulianini. Chromatic detection and discrimination analyzed by a bayesian classifier. *Vision Research*, 41:893–909, 2001.

[53] I. Abramov R.L. DeValois and G.H. Jacobs. Analysis of response patterns of lgn cells. *J. Opt. Soc. Am.*, (56):966–977, 1966.

[54] J. Krauskopf P. Lennie and G. Sclar. Chromatic mechanisms in striate cortex of macaque. *J. Neurosci.*, (10):649–669, 1990.

[55] N. Cottaris R.L. DeValois and S.Elfar. S-cone inputs to striate cortex cells. *Invest. Ophtalmol. Vis. Sci.*, 1997.

[56] S.B. Fenstenmaker D.C. Kiper and K.R. Gegenfurtner. Chromatic properties of neurons in macaque area v2. *Vis. Neuroscience*, (14):1061–1072, 1997.

[57] D.C. Kiper K.R. Gegenfurtner and J.B. Levitt. Functional properties of neurons in macaque area v3. *J. Neurophysiol.*, (77):1906–1923, 1997.

[58] J.S. McLellan R.T. Eskew Jr. and F. Giulianini. *Color Vision from genes to perception*, chapter : Chromatic detection and discrimination, pages 345–368. K.R. Gegenfurtner and L.T. Sharpe Editors, Cambridge University Press, Cambridge, 1998.

[59] R. Penrose. A generalized inverse for matrices. In *Proceedings Cambridge Phil. Soc.*, volume 51, pages 406–413, 1955.

[60] D. I. MacLeod A. Stockman and N. E. Johnson. Spectral sensitivities of the human cones. *J. Opt. Soc. Am. A*, 10(12):2491–2521, 1993.

[61] D. Farnsworth. The farnsworth-munsell 100 hue test; dichotomous tests for colour vision. *J. Opt. Soc. Am.*, (33):586, 1943.

[62] D.G. Pelli. *The effects of visual noise*. PhD thesis, Department of Physiology, Cambridge University, Cambridge, UK, 1981.

[63] D. Karsten G.E. Legge and A.E. Burgess. Contrast discrimination in noise. *J.Opt. Soc. Amer. A*, 4(2):391–404, February 1987.

[64] J.R. Taylor. *An introduction to error analysis*. Oxford University Press, 1982.

[65] P.G. Hoel. *Introduction to mathematical statistics*. John Wiley & Sons, 5th edition, 1984.